INTERNATIONAL JOURNAL FOR NUMERICAL METHODS IN ENGINEERING
Int. J. Numer. Meth. Engng 2002; **53**:2087–2116 (DOI: 10.1002/nme.385)

Meshfree analysis and design sensitivity analysis for shell structures

Nam Ho Kim[1,†], Kyung Kook Choi[1,*,‡], Jiun-Shyan Chen[1,§] and Mark E. Botkin[2,¶]

[1] *Center for Computer-Aided Design and Department of Mechanical Engineering, College of Engineering, University of Iowa, Iowa City, IA 52242, U.S.A.*
[2] *Vehicle Analysis & Dynamics, General Motors R&D and Planning, Mail Code 480-106-256, 30500 Mound Rd. 106, Box 9055, Warren, MI 48090-9055, U.S.A.*

SUMMARY

A unified design sensitivity analysis method for a meshfree shell structure with respect to size, shape, and configuration design variables is presented in this paper. A shear deformable shell formulation is characterized by a CAD connection, thickness degeneration, meshfree discretization, and nodal integration. Because of a strong connection to the CAD tool, the design variable is selected from the CAD parameters, and a consistent design velocity field is then computed by perturbing the surface geometric matrix. The material derivative concept is utilized in order to obtain a design sensitivity equation in the parametric domain. Numerical examples show the accuracy and efficiency of the proposed design sensitivity analysis method compared to the analytical solution and the finite difference solution. Copyright © 2002 John Wiley & Sons, Ltd.

KEY WORDS: mesh-free method; design sensitivity analysis; shell structure; sizing design; shape design; configuration design

1. INTRODUCTION

Among many structural components, a shell is the most frequently used in industrial applications. Especially for automotive and aircraft body structures, the shell component makes up more than 90% of the total structure. Consequently, the design optimization of the shell structure has been an active research area for decades [1]. Even though significant research has been reported for shell structural optimization [2–11], however, the importance of design

*Correspondence to: Kyung Kook Choi, College of Engineering, Center for Computer-Aided Design, 208 Engineering Research Facility, University of Iowa, Iowa City, IA 52242, U.S.A.
† E-mail: nkim@ccad.uiowa.edu
‡ E-mail: kkchoi@ccad.uiowa.edu
§ E-mail: jschen@seas.ucla.edu
¶ E-mail: mark_e._botkin@gmr.com

Contract/grant sponsor: General Motors, Michigan, U.S.A.
Contract/grant sponsor: NSF/DARPA (OPAAL)

Received 2 February 2001
Revised 9 May 2001

sensitivity analysis (DSA) has not been fully uncovered. The finite difference method (FDM) [2–4], the semi-analytical method [5, 6], the discrete method [7, 8], and the continuum method [9–11] have been used to calculate sensitivity information for the shell structure. FDM may be the easiest way to compute sensitivity information. However, this method has major disadvantages from the viewpoint of sensitivity accuracy and computational cost. Because the semi-analytical method uses FDM in part of its sensitivity computation, it has the same disadvantages as FDM [12]. The discrete approach differentiates the finite element (FE) matrix equation with respect to the design variable. However, since the stiffness matrix and the load vector are calculated using the same numerical integration procedure, this discrete derivative may not be easily obtained for general cases, especially when multi-point constraints exist. Moreover, differentiation of the stiffness matrix requires a large amount of computational costs. The continuum method directly differentiates the continuum structure before any discretization. Since no derivative of the stiffness matrix is involved, this approach is more efficient than the discrete method. Theoretically, since the FE matrix equation provides an approximated solution to the continuum problem, it is dangerous to differentiate the approximated problem instead of directly differentiating the continuum problem.

The objective of this paper is to develop a unified design sensitivity formulation for the shell structure with respect to size, shape, and configuration design variables using the meshfree method. The uniqueness of this paper is twofold: (1) to our knowledge, this paper is the first attempt to formulate DSA for a curved shell structure using the meshfree method and (2), by defining the design velocity field on a solid model level, a unified design sensitivity formulation is obtained for all three types of design variables. Given that size, shape, and configuration designs can all be described as a shape design in the solid model, a shape design velocity field is defined on the solid model level, and then degenerated by following the same shell kinematics. Through a seamless integration with a CAD tool, design variables are selected from CAD parameters, and a consistent design velocity field is calculated by perturbing the surface geometric matrix and the shell thickness. By using a degenerated design velocity field, the continuum structural equation is differentiated in order to obtain a unified design sensitivity equation in the parametric domain.

A main challenge in shell formulation is the inability to model thin structures due to the lack of a bending and an in-extensional mode. This difficulty is often referred to as shear and membrane locking. Many numerical schemes have been proposed to resolve numerical locking in FE-based approaches, including the selective reduced integration method [13], the $\bar{B}$ method [14], the mixed formulation [15], the assumed strain method [16], and the discrete Kirchhoff approach [17]. Several research results also have been reported in the plate/shell formulation by using the meshfree method. Initially, Krysl and Belytschko [18] developed a thin plate/shell formulation using the element-free Galerkin method. Donning and Liu [19] proposed a locking-free shear-deformable plate formulation. Recently, Garcia *et al*. [20] shows that shear locking can be controlled by using sufficiently high-order polynomials in hp-clouds. Noguchi *et al*. [21] extended the element-free Galerkin method to the general curved shell structure by using a mapping to the convected co-ordinate.

In this paper, a shear-deformable shell formulation is proposed, with the characteristics of a CAD connection, thickness degeneration, meshfree discretization, and nodal integration. A seamless integration with a CAD tool provides a better approximation of the shell structure, including the surface normal vector and mapping relation. A meshfree shape function is constructed in the parametric domain that has been obtained from the CAD tool. Since the

meshfree interpolation function is constructed in the parametric domain, it is shown that the interpolation function is independent of design variables. A stabilized conforming (SC) nodal integration method, which is developed by Chen *et al.* [22], is used to resolve the locking difficulty in the meshfree shell formulation. This SC nodal integration also allows for a significant reduction of computational time in meshfree analysis and thus in DSA. The integration zone concept originally employed in the conventional meshfree method [23] is eliminated.

The organization of this paper is as follows. After a parametric representation of the shell surface within the CAD tool is introduced in Section 2, a variational formulation of the shell structure is developed in Section 3. In Section 4, a shear-deformable meshfree shell formulation is presented in conjunction with the SC nodal integration. A unified design sensitivity formulation is developed in Section 5, followed by numerical examples in Section 6, in which the accuracy and efficiency of the proposed sensitivity result is compared to the analytical solution and the finite difference solution.

2. CAD-BASED GEOMETRIC MAPPING

A general shell structure can be represented by a neutral surface geometry and thickness data at each point. A surface component in a CAD tool is well-served for this purpose, and is frequently used to generate a shell element in FEA. Since no element information is generated for the meshfree method, it is necessary to use the information from the CAD tool, especially for constructing the surface normal vector and mapping from the global co-ordinate to the local co-ordinate system.

In the CAD tool, a surface geometry $\mathbf{x}^n$ in a general, three-dimensional space can be represented by using two parameters as

$$\mathbf{x}^n(\xi,\eta) = \mathbf{U}(\xi)^{\mathrm{T}}\mathbf{M}\mathbf{G}\mathbf{M}^{\mathrm{T}}\mathbf{W}(\eta) \tag{1}$$

where $\mathbf{U}(\xi) = [\xi^3, \xi^2, \xi, 1]^{\mathrm{T}}$ and $\mathbf{W}(\eta) = [\eta^3, \eta^2, \eta, 1]^{\mathrm{T}}$ are vectors in the parametric co-ordinates, $\mathbf{M}$ is the matrix defined as

$$\mathbf{M} = \begin{bmatrix} 2 & -2 & 1 & 1 \\ -3 & 3 & -2 & -1 \\ 0 & 0 & 1 & 0 \\ 1 & 0 & 0 & 0 \end{bmatrix} \tag{2}$$

and $\mathbf{G}$ is the surface geometric matrix defined as

$$\mathbf{G} = \begin{bmatrix} \mathbf{p}_{00} & \mathbf{p}_{01} & \mathbf{p}_{00}^{\eta} & \mathbf{p}_{01}^{\eta} \\ \mathbf{p}_{10} & \mathbf{p}_{11} & \mathbf{p}_{10}^{\eta} & \mathbf{p}_{11}^{\eta} \\ \mathbf{p}_{00}^{\xi} & \mathbf{p}_{01}^{\xi} & \mathbf{p}_{00}^{\xi\eta} & \mathbf{p}_{01}^{\xi\eta} \\ \mathbf{p}_{10}^{\xi} & \mathbf{p}_{11}^{\xi} & \mathbf{p}_{10}^{\xi\eta} & \mathbf{p}_{11}^{\xi\eta} \end{bmatrix}_{4\times4\times3} \tag{3}$$

where $\mathbf{p}_{ij}$ are co-ordinates of the corner points on the surface, $\mathbf{p}_{ij}^{\xi}$ and $\mathbf{p}_{ij}^{\eta}$ are the tangent vectors in ξ and η directions, and $\mathbf{p}_{ij}^{\xi\eta}$ are the twist vectors. Equation (1) relates the physical

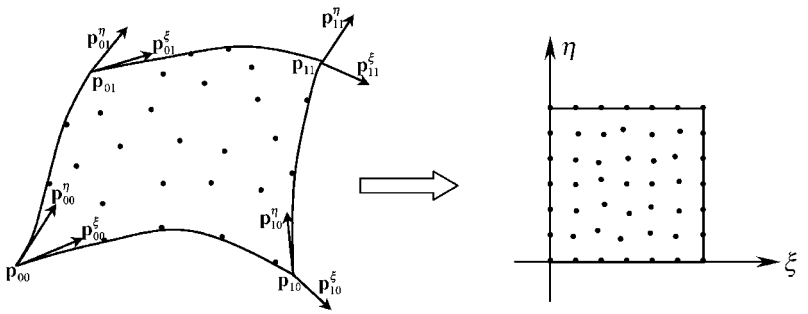

Figure 1. Parametric representation of a surface geometry.

co-ordinate $\mathbf{x}^n$ to the parametric co-ordinate (ξ, η). Figure 1 shows the surface geometry and its transformation into the parametric co-ordinate. The surface representation method in Equation (1) is well known with parametric modeling technology [24, 25].

The surface representation scheme in Equation (1) provides a great amount of flexibility from a computational viewpoint. For example, the unit normal vector on the surface at (ξ, η) can be obtained as

$$\mathbf{n}(\xi, \eta) = \frac{\mathbf{x}^n_{,\xi} \times \mathbf{x}^n_{,\eta}}{\|\mathbf{x}^n_{,\xi} \times \mathbf{x}^n_{,\eta}\|} \tag{4}$$

where, from Equation (1),

$$\mathbf{x}^n_{,\xi} = \mathbf{U}^{\mathrm{T}}_{,\xi}(\xi)\mathbf{M}\mathbf{G}\mathbf{M}^{\mathrm{T}}\mathbf{W}(\eta) \tag{5}$$

$$\mathbf{x}^n_{,\eta} = \mathbf{U}(\xi)^{\mathrm{T}}\mathbf{M}\mathbf{G}\mathbf{M}^{\mathrm{T}}\mathbf{W}_{,\eta}(\eta) \tag{6}$$

The surface normal vector in Equation (4) reduces a significant amount of discretization error that often occurs in the traditional FEA.

In the shell formulation, the surface representation in Equation (1) yields the co-ordinate of the neutral surface. If a shell structure is considered as a degenerated solid component, then a complete mapping relation between the physical co-ordinate and the parametric co-ordinate can be obtained. For a shell structure with thickness $t(\xi, \eta)$, any points within the structure can be expressed by

$$\mathbf{x}(\xi, \eta, \zeta) = \mathbf{U}(\xi)^{\mathrm{T}}\mathbf{M}\mathbf{G}\mathbf{M}^{\mathrm{T}}\mathbf{W}(\eta) + \zeta\frac{t}{2}\mathbf{n}(\xi, \eta) \tag{7}$$

where $\zeta = [-1, 1]$ is the third parametric co-ordinate in the thickness direction, and $\mathbf{n}(\xi, \eta)$ is the outward unit normal vector of the surface, obtained from Equation (4). In Equation (7) the neutral surface is presumed to be the mid-surface. However, this assumption can be eliminated without significant technical complication. The Jacobian of the mapping relation

can be obtained, from the relation in Equation (7), as

$$\begin{aligned} \mathbf{x}_{,\xi} &= \mathbf{U}^{\mathrm{T}}_{,\xi}\mathbf{M}\mathbf{G}\mathbf{M}^{\mathrm{T}}\mathbf{W} + \zeta\frac{t}{2}\mathbf{n}_{,\xi} \\ \mathbf{x}_{,\eta} &= \mathbf{U}^{\mathrm{T}}\mathbf{M}\mathbf{G}\mathbf{M}^{\mathrm{T}}\mathbf{W}_{,\eta} + \zeta\frac{t}{2}\mathbf{n}_{,\eta} \\ \mathbf{x}_{,\zeta} &= \frac{t}{2}\mathbf{n} \end{aligned} \tag{8}$$

The notations $\mathbf{x} = [x, y, z]^{\mathrm{T}} = [x_1, x_2, x_3]^{\mathrm{T}}$ and $\boldsymbol{\xi} = [\xi, \eta, \zeta]^{\mathrm{T}} = [\xi_1, \xi_2, \xi_3]^{\mathrm{T}}$ will be used for the following derivations whenever appropriate. Using these notations, the Jacobian of the mapping can be represented by

$$\mathbf{J} = \frac{\partial x_i}{\partial \xi_j} \tag{9}$$

Since a one-to-one mapping relation is preserved in Equation (7), the Jacobian matrix in Equation (9) is nonsingular and thus its inverse $\mathbf{J}^{-1}$ exists.

In conjunction with meshfree discretization, which will be introduced in Section 4, the CAD-based geometric representation method in Equation (7) provides a better approximation of the continuum shell structure. The curvature of the shell structure is well-represented, without approximating it. Thus, geometric simplification is avoided in this approach.

In the shell structure, the constitutive relation is given in the body-fixed, local co-ordinate system, whereas a displacement–strain relation is provided in the global co-ordinate system. Thus, a transformation between the local and global co-ordinates is required. In this paper, since a parametric representation of the shell surface is available, the following relation is used for the co-ordinate transformation:

$$\mathbf{l} = \frac{\mathbf{x}^n_{,\xi}}{\|\mathbf{x}^n_{,\xi}\|}, \quad \mathbf{n} = \frac{\mathbf{x}^n_{,\xi} \times \mathbf{x}^n_{,\eta}}{\|\mathbf{x}^n_{,\xi} \times \mathbf{x}^n_{,\eta}\|}, \quad \mathbf{m} = \mathbf{n} \times \mathbf{l} \tag{10}$$

$$\mathbf{x} = \begin{bmatrix} l_1 & m_1 & n_1 \\ l_2 & m_2 & n_2 \\ l_3 & m_3 & n_3 \end{bmatrix} \mathbf{x}' \tag{11}$$

where $\mathbf{x}'$ is the co-ordinate of $\mathbf{x}$ in the body-fixed co-ordinate system. The local co-ordinate is constructed such that the x'_1-axis is parallel to the $\mathbf{l}$ vector, and the x'_3-axis is parallel to the $\mathbf{n}$ vector.

3. VARIATIONAL FORMULATION FOR THE SHELL STRUCTURE

A variational formulation for the shell structure is obtained by degenerating the three-dimensional solid component in the continuum domain. Given the assumption of a constant transverse shear deformation, analytical integration can be performed through the thickness co-ordinate.

The strain tensor in linear elasticity can be expressed as

$$\varepsilon_{ij}(\mathbf{z}) = \frac{1}{2}\left(\frac{\partial z_i}{\partial x_j} + \frac{\partial z_j}{\partial x_i}\right) = \mathrm{sym}(z_{i,j}) \tag{12}$$

where sym($\bullet$) denotes the symmetric part of the tensor, and the subscript after the comma represents the derivative with respect to the spatial co-ordinate. If the parametric co-ordinate introduced in the previous section is used to represent the strain tensor in Equation (12), then we have

$$\varepsilon_{ij}(\mathbf{z}) = \frac{1}{2}\left(\frac{\partial z_i}{\partial \xi_m}\frac{\partial \xi_m}{\partial x_j} + \frac{\partial z_j}{\partial \xi_m}\frac{\partial \xi_m}{\partial x_i}\right) = \mathrm{sym}\left(\frac{\partial z_i}{\partial \xi_m} J^{-1}_{mj}\right) \tag{13}$$

where the summation rule is used for the repeated indices.

The variational formulation for the structure can be obtained either from the principle of virtual work, or from the principle of minimum total potential energy [26]. If we let the structural domain be $\Omega \subset R^3$, and the corresponding parametric domain be $\Omega^r \times R$, $\Omega^r \subset R^2$, then the structural energy form for linear elasticity can be obtained as

$$\begin{aligned} a(\mathbf{z}, \bar{\mathbf{z}}) &= \iiint_{\Omega} \varepsilon_{ij}(\bar{\mathbf{z}}) C_{ijkl} \varepsilon_{kl}(\mathbf{z})\, \mathrm{d}\Omega \\ &= \iiint_{\Omega^r \times R} \mathrm{sym}\left(\frac{\partial z_i}{\partial \xi_m} J^{-1}_{mj}\right) C_{ijkl}\, \mathrm{sym}\left(\frac{\partial z_j}{\partial \xi_n} \mathrm{J}^{-1}_{ni}\right) |J|\, \mathrm{d}\xi_1\, \mathrm{d}\xi_2\, \mathrm{d}\xi_3 \end{aligned} \tag{14}$$

where $\bar{\mathbf{z}}$ denotes the displacement variation or the virtual displacement, C_{ijkl} the fourth-order constitutive tensor, Ω^r the (ξ, η) plane, and $|\mathbf{J}|$ the determinant of the Jacobian in Equation (9).

To further simplify the structural energy form, let us assume that displacement varies linearly in the thickness direction. This assumption yields a similar result as a Mindlin–Reissner shell formulation [27, 28], in which the flat cross-section remains flat during deformation. Accordingly, the displacement is a linear function of ζ and can be represented by the addition of two terms as

$$\mathbf{z} = \mathbf{z}^1(\xi, \eta) + \zeta \mathbf{z}^2(\xi, \eta) \tag{15}$$

where $\mathbf{z}^1(\xi, \eta)$ represents the displacement of the neutral surface (the membrane deformation) and $\zeta \mathbf{z}^2(\xi, \eta)$ denotes the rotation of the cross-section (the bending and shear deformation). In addition, since the dimension of the thickness direction is much smaller than that of the others, Jacobian $\mathbf{J}$ can be presumed to be a function of only ξ and η co-ordinates. Accordingly, given the linear property of the engineering strain, the strain tensor in Equation (13) can also be represented by the addition of two terms

$$\varepsilon_{ij}(\mathbf{z}) = \varepsilon^1_{ij}(\mathbf{z}) + \zeta \varepsilon^2_{ij}(\mathbf{z}) \tag{16}$$

where

$$\varepsilon^1_{ij}(\mathbf{z}) = \mathrm{sym}\left(\frac{\partial z^1_i}{\partial \xi_m} J^{-1}_{mj} + z^2_i J^{-1}_{3j}\right) \tag{17}$$

$$\varepsilon_{ij}^2(\mathbf{z}) = \mathrm{sym}\left(\frac{\partial z_i^2}{\partial \xi_m} J_{mj}^{-1}\right) \tag{18}$$

are the membrane–shear strain and bending strain, respectively. Unlike the Mindlin–Reissner plate formulation, the membrane and transverse shear strains are coupled in Equation (17).

It is clear from the aforementioned assumptions that the structural energy form in Equation (14) is a quadratic function of the parametric co-ordinate ζ. After analytically integrating Equation (14) over the interval $\zeta \in [-1, 1]$, the structural energy form is simplified as

$$a(\mathbf{z}, \bar{\mathbf{z}}) = 2 \iint_{\Omega^r} \varepsilon_{ij}^1(\bar{\mathbf{z}}) C_{ijkl} \varepsilon_{kl}^1(\mathbf{z}) |\mathbf{J}| \, \mathrm{d}\Omega^r + \frac{2}{3} \iint_{\Omega^r} \varepsilon_{ij}^2(\bar{\mathbf{z}}) C_{ijkl} \varepsilon_{kl}^2(\mathbf{z}) |\mathbf{J}| \, \mathrm{d}\Omega^r \tag{19}$$

Note that the coupled terms of $\varepsilon_{ij}^1(\mathbf{z})$ and $\varepsilon_{ij}^2(\mathbf{z})$ vanish since they are odd functions of ζ. The degenerated structural energy form in Equation (19) is still based on the continuum domain, and domain discretization has not yet been introduced. Since the analytical integration is already carried out over parametric co-ordinate ζ, only the domain discretization of the neutral surface is necessary.

If a conservative system were considered, then the applied load would be independent of deformation. If we let $\mathbf{f}^{\mathrm{B}}$ be the body force per unit volume, then the load linear form can be written as

$$\ell(\bar{\mathbf{z}}) = \iiint_{\Omega} \bar{\mathbf{z}}^{\mathrm{T}} \mathbf{f}^{\mathrm{B}} \, \mathrm{d}\Omega \tag{20}$$

After introducing the parametric co-ordinate and integrating Equation (20) along the ζ-axis, we obtain

$$\ell(\bar{\mathbf{z}}) = 2 \iint_{\Omega^r} \bar{\mathbf{z}}^{\mathrm{T}} \mathbf{f}^{\mathrm{B}} |\mathbf{J}| \, \mathrm{d}\Omega^r \tag{21}$$

For simplicity of explanation, the traction force will not be considered in Equation (21).

The structural equilibrium equation can be obtained from Equations (19) and (21). For a given $\mathbf{f}^{\mathrm{B}}$ and Γ_h, the structural variational equation is

$$a(\mathbf{z}, \bar{\mathbf{z}}) = \ell(\bar{\mathbf{z}}), \quad \forall \bar{\mathbf{z}} \in Z \tag{22}$$

In Equation (22), the space Z of kinematically admissible displacements is defined as

$$Z = \{\mathbf{w} \in [H^1(\Omega)]^3 \mid \mathbf{w}(\mathbf{x}) = 0 \text{ on } \mathbf{x} \in \Gamma_h\} \tag{23}$$

where $H^1(\Omega)$ is the Sobolev space of order one, and Γ_h is the essential boundary in which the displacement is prescribed. The continuum form of variational Equation (22) will be discretized in the following section using the meshfree method.

4. SHEAR-DEFORMABLE MESHFREE SHELL FORMULATION

Two numerical procedures are required in order to solve the variational Equation (22): the interpolation method for the state variable (displacement) and the domain integration method. The finite element method approximates the state variable within an element by using piecewise polynomials, and as a result, this approximation inevitably depends on the finite element

Figure 2. Types of kernel functions: (a) hat shape; (b) cap shape, and (c) bell shape.

shape. In addition, since the Gauss integration method maps the finite element onto the reference element, the Jacobian matrix for the mapping depends on the finite element shape.

In the meshfree method, the state variable is approximated by using a supporting set of particles in the global sense. Combined with the SC nodal integration method, the meshfree method can remove mesh-dependent interpolation and integration accuracy problems. Although in the initial development the meshfree shape function is constructed from the global particle distribution, a modified approach is used in this paper, such that the meshfree shape function is constructed in the parametric space.

4.1. Review of the meshfree method

In the meshfree method, the parametric domain Ω^r of the structure is discretized by an NP number of particle points. It is not necessary to specify the connectivity of these particles except for those on the boundary Γ. For simplicity, let $z(\boldsymbol{\xi})$ be a scalar state variable, which is the solution to the structural problem. The reproducing kernel (RK) approximation of $z(\boldsymbol{\xi})$ is [23]

$$z^{\mathrm{R}}(\boldsymbol{\xi}) = \sum_{I=1}^{NP} \Psi_I(\boldsymbol{\xi}) d_I \tag{24}$$

where d_I is the approximation coefficient corresponding to the particle point $\boldsymbol{\xi}_I$ and $\Psi_I(\boldsymbol{\xi})$ is the meshfree shape function. $\Psi_I(\boldsymbol{\xi})$ is constructed from the smoothness requirement and the completeness condition [22]. In this paper, the cubic spline function and the second-order completeness condition are considered, in which the approximation in Equation (24) is exact up to and including the quadratic field.

In the RK approximation, the shape function in Equation (24) is constructed as

$$\Psi_I(\boldsymbol{\xi}) = C(\boldsymbol{\xi}; \boldsymbol{\xi} - \boldsymbol{\xi}_I)\phi_a(\boldsymbol{\xi} - \boldsymbol{\xi}_I) \tag{25}$$

where $\phi_a(\boldsymbol{\xi})$ is a kernel (window) function that covers all particles within compact support size 'a' and $C(\boldsymbol{\xi}; \boldsymbol{\xi} - \boldsymbol{\xi}_I)$ is a correction function. The smoothness of the shape function is controlled by $\phi_a(\boldsymbol{\xi})$, which is non-zero within $[-a, a]$. Each particle point has a specific size of compact support 'a', which can be viewed as the affected region. The general shape of $\phi_a(\boldsymbol{\xi})$ is shown in Figure 2. For the general two-dimensional parametric domain Ω^r, the kernel function of Figure 2 in each co-ordinate frame is multiplied to obtain

$$\phi_a(\boldsymbol{\xi} - \boldsymbol{\xi}_I) = \phi_a(\xi_1 - \xi_{I1})\phi_a(\xi_2 - \xi_{I2}) \tag{26}$$

Note that the non-zero region of the shape function is limited to within the compact support of the kernel function. Thus, the summation in Equation (24) need not be carried out over

the entire *NP* number of particles. If *IP* is the number of particles in which the support size covers, then the summation is carried out over the *IP* number of particles.

The correction function in Equation (25) is obtained from the requirement of representing a zero-, first-, and second-order polynomial, exactly. Let $C(\xi;\xi-\xi_I)$ be constructed by a linear combination of complete, second-order monomial bases as

$$C(\xi;\xi-\xi_I)=\mathbf{H}^{\mathrm{T}}(\xi-\xi_I)\mathbf{q}(\xi) \tag{27}$$

where

$$\mathbf{H}(\xi-\xi_I)=\begin{bmatrix}1\\ \xi-\xi_I\\ \eta-\eta_I\\ (\xi-\xi_I)^2\\ (\xi-\xi_I)(\eta-\eta_I)\\ (\eta-\eta_I)^2\end{bmatrix} \tag{28}$$

$\mathbf{H}(\xi-\xi_I)$ is the vector of monomial bases and $\mathbf{q}(\xi)=[q_1, q_2, q_3, q_4, q_5, q_6]^{\mathrm{T}}$ is the coefficient vector. The reproducing condition calculates the coefficient vector $\mathbf{q}(\xi)$, such that the interpolation in Equation (24) is exact up to and including the second-order derivatives of function $z^{\mathrm{R}}(\xi)$, which becomes a system of 6×6 matrix equations as

$$\mathbf{M}(\xi)\mathbf{q}(\xi)=\mathbf{H}(\mathbf{0}) \tag{29}$$

where

$$\mathbf{M}(\xi)=\sum_{I=1}^{IP}\mathbf{H}(\xi-\xi_I)\mathbf{H}^{\mathrm{T}}(\xi-\xi_I)\phi_a(\xi-\xi_I) \tag{30}$$

By substituting solution $\mathbf{q}(\xi)$ from Equation (29) into Equation (27), the correction function can be calculated, provided that $\mathbf{M}(\xi)$ is non-singular. The compact support size 'a' has to be chosen to guarantee the positive definiteness of $\mathbf{M}(\xi)$, which is related to the order of basis function $\mathbf{H}(\xi-\xi_I)$ and the particle distribution density.

The RK approximation of state variable $z(\xi)$ is obtained by substituting the correction function in Equation (27) into Equation (25) as

$$\begin{aligned} z(\xi)&=\sum_{I=1}^{IP}\mathbf{H}^{\mathrm{T}}(\mathbf{0})\mathbf{M}^{-1}(\xi-\xi_I)\mathbf{H}(\xi-\xi_I)\phi_a(\xi-\xi_I)d_I\\ &=\sum_{I=1}^{IP}\Psi_I(\xi)d_I \end{aligned} \tag{31}$$

When the monomial basis function $\mathbf{H}(\xi-\xi_I)$ in Equation (28) is used in the RK approximation, the smoothness and compact support properties of shape function $\Psi_I(\xi)$ are identical to those of the kernel function $\phi_a(\xi-\xi_I)$.

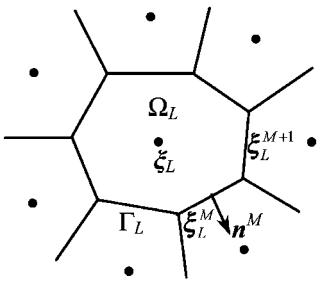

Figure 3. Voronoi diagram of the scattered particle set.

4.2. Strain smoothening and nodal integration

In addition to the construction of the shape function, the solution of the meshfree Galerkin method depends on domain integration. For integration purposes, an initial development of the meshfree method based on Gauss integration requires background meshes. Thus, the subdomain concept in the finite element method still remains. In contrast, the direct nodal integration method experiences a lack of stability, because this method inherits a reduced integration. Recently, Chen *et al.* [22] proposed an SC nodal integration method by imposing an integration constraint to satisfy linear exactness, and by smoothening strain to achieve solution stability. In this section, a SC nodal integration method will be briefly introduced, while detailed information can be found in Chen *et al.* [22].

Strain smoothening is frequently used as a regularization tool for the high strain gradient problem. The instability associated with nodal integration can be resolved by using this approach. In nodal integration, the total structural area is distributed to each particle point, which serves as an integration weight. There are several ways of assigning a nodal area, for example, by using a Voronoi diagram, as shown in Figure 3. Let Ω_L be the nodal domain associated with particle point ξ_L with Γ_L as its boundary. A simple method for strain smoothening is to average over a given area as

$$z_{i,j}^S(\xi_L) = \frac{1}{A_L} \iint_{\Omega_L} z_{i,j} \, \mathrm{d}\Omega \tag{32}$$

where A_L is the area of Ω_L. The domain integration in Equation (32) can then be transformed into a boundary integration by using the divergence theorem as

$$z_{i,j}^S(\xi_L) = \frac{1}{A_L} \int_{\Gamma_L} z_i n_j \, \mathrm{d}\Gamma \tag{33}$$

where **n** is the outward unit normal vector at the boundary. Note that the smoothed strain in Equation (33) contains the displacement and the normal vector at the boundary. In addition, Chen *et al.* [22] showed that the smoothed strain in Equation (33) satisfies the integration constraint such that it can exactly represent a linear field.

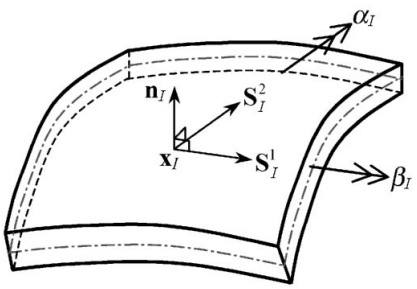

Figure 4. Curved shell geometry.

If boundary Γ_L of the nodal volume in Figure 3 is composed of piecewise linear segments, then a simple trapezoidal rule may be used for each segment of boundary Γ_L as

$$z_{i,j}^S(\boldsymbol{\xi}_L) = \frac{1}{A_L}\sum_{I=1}^{IP}\int_{\Gamma_L}\Psi_I(\boldsymbol{\xi})d_{Ii}n_j(\boldsymbol{\xi})\,\mathrm{d}\Gamma$$
$$= \frac{1}{A_L}\sum_{I=1}^{IP}\sum_{M=1}^{NS}\frac{1}{2}l^M n_j^M(\Psi_I(\boldsymbol{\xi}_L^{M+1}) + \Psi_I(\boldsymbol{\xi}_L^M))d_{Ii} \tag{34}$$

where l^M is the length of the Mth boundary segment, and NS is the number of closed boundary segments associated with $\boldsymbol{\xi}_L$. Thus, the strain computation is related to the evaluation of the meshfree shape functions at each corner of the nodal domain. The smoothed strain in Equation (33) is used in the following discretization, without the inclusion of superscript S for the sake of simplicity.

4.3. Discretization of the shear-deformable shell structure

From Equation (31), the displacement at the parametric location (ξ, η, ζ) can be approximated by using the meshfree interpolation function and the generalized response variables as

$$\mathbf{z}(\xi,\eta,\zeta) = \sum_{I=1}^{IP}\Psi_I(\xi,\eta)\mathbf{d}_I + \sum_{I=1}^{IP}\Psi_I(\xi,\eta)\frac{t_I}{2}\zeta[\mathbf{S}_I^{1^{\mathrm{T}}}, -\mathbf{S}_I^{2^{\mathrm{T}}}]\begin{bmatrix}\alpha_I\\ \beta_I\end{bmatrix}$$
$$\equiv \sum_{I=1}^{IP}\mathbf{N}_I(\xi,\eta,\zeta)\mathbf{r}_I \equiv \mathbf{A}\mathbf{r} \tag{35}$$

where $\mathbf{r}, = [\mathbf{r}_1^{\mathrm{T}}, \mathbf{r}_2^{\mathrm{T}}, \ldots, \mathbf{r}_{NP}^{\mathrm{T}}]^{\mathrm{T}}$, $\mathbf{r}_I = [d_{I1}, d_{I2}, d_{I3}, \alpha_I, \beta_I]^T$, $\mathbf{d}_I = [d_{I1}, d_{I2}, d_{I3}]^{\mathrm{T}}$ is the generalized displacement vector, and α_I and β_I are the generalized rotational vectors with respect to the direction of $\mathbf{S}_I^2$ and $\mathbf{S}_I^1$, respectively (see Figure 4). $\mathbf{S}_I^2$ and $\mathbf{S}_I^1$ can be defined as follows:

$$\begin{aligned}\mathbf{S}_I^1 &= \mathbf{n}_I \times \mathbf{e}_1\\ \mathbf{S}_I^2 &= \mathbf{n}_I \times \mathbf{S}_I^1\end{aligned} \tag{36}$$

where $\mathbf{e}_1 = [1,0,0]^{\mathrm{T}}$ is the x-directional unit vector in the global co-ordinate. When $\mathbf{n}_I$ is parallel to $\mathbf{e}_1$, then one can simply established that $\mathbf{S}_I^1 = \mathbf{e}_1$. As discussed in Section 4.1, the generalized response variable $\mathbf{r}_I$ is not nodal values. If Equation (35) is compared with Equation (15), then it is clear that the first summation corresponds to $\mathbf{z}^1(\xi,\eta)$ and the second summation represents $\zeta\mathbf{z}^2(\xi,\eta)$.

To obtain the discretized strain vector in Equation (13), the derivative of $\mathbf{z}$ with respect to the parametric co-ordinate is calculated first from the relation in Equation (35) as

$$\left[\frac{\partial z_i}{\partial \xi_j}\right]_{9\times 1} = \sum_{I=1}^{IP} \mathbf{G}_I^1 \mathbf{r}_I + \zeta \sum_{I=1}^{IP} \mathbf{G}_I^2 \mathbf{r}_I \tag{37}$$

where

$$\mathbf{G}_I^1 = \begin{bmatrix} \Psi_{I,\xi} & 0 & 0 & 0 & 0 \\ \Psi_{I,\eta} & 0 & 0 & 0 & 0 \\ 0 & 0 & 0 & \frac{1}{2}\Psi_I t_I S_{Ix}^1 & -\frac{1}{2}\Psi_I t_I S_{Ix}^2 \\ 0 & \Psi_{I,\xi} & 0 & 0 & 0 \\ 0 & \Psi_{I,\eta} & 0 & 0 & 0 \\ 0 & 0 & 0 & \frac{1}{2}\Psi_I t_I S_{Iy}^1 & -\frac{1}{2}\Psi_I t_I S_{Iy}^2 \\ 0 & 0 & \Psi_{I,\xi} & 0 & 0 \\ 0 & 0 & \Psi_{I,\eta} & 0 & 0 \\ 0 & 0 & 0 & \frac{1}{2}\Psi_I t_I S_{Iz}^1 & -\frac{1}{2}\Psi_I t_I S_{Iz}^2 \end{bmatrix} \tag{38}$$

is the contribution from the membrane and transverse shear parts, and

$$\mathbf{G}_I^2 = \begin{bmatrix} 0 & 0 & 0 & \frac{1}{2}\Psi_{I,\xi} t_I S_{Ix}^1 & -\frac{1}{2}\Psi_{I,\xi} t_I S_{Ix}^2 \\ 0 & 0 & 0 & \frac{1}{2}\Psi_{I,\eta} t_I S_{Ix}^1 & -\frac{1}{2}\Psi_{I,\eta} t_I S_{Ix}^2 \\ 0 & 0 & 0 & 0 & 0 \\ 0 & 0 & 0 & \frac{1}{2}\Psi_{I,\xi} t_I S_{Iy}^1 & -\frac{1}{2}\Psi_{I,\xi} t_I S_{Iy}^2 \\ 0 & 0 & 0 & \frac{1}{2}\Psi_{I,\eta} t_I S_{Iy}^1 & -\frac{1}{2}\Psi_{I,\eta} t_I S_{Iy}^2 \\ 0 & 0 & 0 & 0 & 0 \\ 0 & 0 & 0 & \frac{1}{2}\Psi_{I,\xi} t_I S_{Iz}^1 & -\frac{1}{2}\Psi_{I,\xi} t_I S_{Iz}^2 \\ 0 & 0 & 0 & \frac{1}{2}\Psi_{I,\eta} t_I S_{Iz}^1 & -\frac{1}{2}\Psi_{I,\eta} t_I S_{Iz}^2 \\ 0 & 0 & 0 & 0 & 0 \end{bmatrix} \tag{39}$$

is the contribution from the bending part. In Equation (37), a vector notation is used for convenience, such that $\partial z_i/\partial \xi_j$ is the 9×1 column vector.

As shown in Equation (13), the strain in the spatial co-ordinate is transformed into the parametric co-ordinate by using Equation (37) as

$$\boldsymbol{\varepsilon}(\mathbf{x}_L;\mathbf{z}) = \begin{Bmatrix} z_{1,1} \\ z_{2,2} \\ z_{3,3} \\ z_{1,2}+z_{2,1} \\ z_{2,3}+z_{3,2} \\ z_{1,3}+z_{3,1} \end{Bmatrix} = \mathbf{S}_q\mathbf{T}\sum_{I=1}^{IP}(\mathbf{G}_I^1\mathbf{r}_I+\zeta\mathbf{G}_I^2\mathbf{r}_I) \equiv \sum_{I=1}^{IP}[\mathbf{B}_I^1(\mathbf{x}_L)\mathbf{r}_I+\zeta\mathbf{B}_I^2(\mathbf{x}_L)\mathbf{r}_I] \tag{40}$$

where $\mathbf{T}$ is the 9×9 mapping matrix

$$\mathbf{T}_I = \begin{bmatrix} \mathbf{J}_{3\times 3}^{-1} & \mathbf{0} & \mathbf{0} \\ \mathbf{0} & \mathbf{J}_{3\times 3}^{-1} & \mathbf{0} \\ \mathbf{0} & \mathbf{0} & \mathbf{J}_{3\times 3}^{-1} \end{bmatrix}_I \tag{41}$$

and where

$$\mathbf{S}_q = \begin{bmatrix} 1 & 0 & 0 & 0 & 0 & 0 & 0 & 0 & 0 \\ 0 & 0 & 0 & 0 & 1 & 0 & 0 & 0 & 0 \\ 0 & 0 & 0 & 0 & 0 & 0 & 0 & 0 & 1 \\ 0 & 1 & 0 & 1 & 0 & 0 & 0 & 0 & 0 \\ 0 & 0 & 0 & 0 & 0 & 1 & 0 & 1 & 0 \\ 0 & 0 & 1 & 0 & 0 & 0 & 1 & 0 & 0 \end{bmatrix} \tag{42}$$

In Equation (40), $\mathbf{B}_I^1$ and $\mathbf{B}_I^2$ are the strain–displacement matrices for the membrane–shear part and the bending part, respectively.

For the linear elastic material, the stiffness matrix in the body-fixed co-ordinate system can be given as

$$\mathbf{D} = \frac{E}{(1-v^2)}\begin{bmatrix} 1 & v & 0 & 0 & 0 & 0 \\ v & 1 & 0 & 0 & 0 & 0 \\ 0 & 0 & 0 & 0 & 0 & 0 \\ 0 & 0 & 0 & \dfrac{1-v}{2} & 0 & 0 \\ 0 & 0 & 0 & 0 & \kappa\dfrac{1-v}{2} & 0 \\ 0 & 0 & 0 & 0 & 0 & \kappa\dfrac{1-v}{2} \end{bmatrix} \tag{43}$$

where E is Young's modulus, v is Poisson's ratio, and $\kappa = 5/6$ is the shear correction factor. Since the stiffness matrix in Equation (43) is constructed in the body-fixed local co-ordinate system, $\mathbf{D}$ must be transformed in order to fit into the global co-ordinate system, where the strain–displacement matrix of Equation (40) is defined. This transformation can be found in

the literature, as in the example of Bathe [29], and written as

$$\mathbf{C} = \mathbf{Q}^{\mathrm{T}}\mathbf{D}\mathbf{Q} \tag{44}$$

where

$$\mathbf{Q} = \begin{bmatrix} l_1^2 & m_1^2 & n_1^2 & l_1 m_1 & m_1 n_1 & n_1 l_1 \\ l_2^2 & m_2^2 & n_2^2 & l_2 m_2 & m_2 n_2 & n_2 l_2 \\ l_3^2 & m_3^2 & n_3^2 & l_3 m_3 & m_3 n_3 & n_3 l_3 \\ 2l_1 l_2 & 2m_1 m_2 & 2n_1 n_2 & l_1 m_2 + l_2 m_1 & m_1 n_2 + m_2 n_1 & n_1 l_2 + n_2 l_1 \\ 2l_2 l_3 & 2m_2 m_3 & 2n_2 n_3 & l_2 m_3 + l_3 m_2 & m_2 n_3 + m_3 n_2 & n_2 l_3 + n_3 l_2 \\ 2l_3 l_1 & 2m_3 m_1 & 2n_3 n_1 & l_3 m_1 + l_1 m_3 & m_3 n_1 + m_1 n_3 & n_3 l_1 + n_1 l_3 \end{bmatrix} \tag{45}$$

The structural energy form in Equation (19) and the load linear form in Equation (21) can be discretized with the meshfree shape function and the SC nodal integration scheme, to arrive at

$$a(\mathbf{z}, \bar{\mathbf{z}}) \approx \bar{\mathbf{r}}^{\mathrm{T}}\mathbf{K}\mathbf{r} \tag{46}$$

$$\ell(\bar{\mathbf{z}}) \approx \bar{\mathbf{r}}^{\mathrm{T}}\mathbf{F} \tag{47}$$

where $\bar{\mathbf{r}}$ is the virtual displacement vector, and

$$\mathbf{K} = \sum_{L=1}^{NP} (\mathbf{K}_L^1 + \mathbf{K}_L^2) \tag{48}$$

$$\mathbf{F} = \sum_{L=1}^{NP} \mathbf{F}_L \tag{49}$$

are the stiffness matrix and external load vector, respectively. The external load vector in Equation (49) is computed from its continuum form in Equation (21) as

$$\mathbf{F}_L = \mathbf{L}\left\{ \sum_{I=1}^{IP} 2\Psi_I \mathbf{f}^{\mathrm{B}}(\mathbf{x}_L)|\mathbf{J}|A_L \right\} \tag{50}$$

where $\mathbf{L}\{\,\}$ represents the assembly procedure. The stiffness matrix of the problem has two different components from Equation (19),

$$[\mathbf{K}_L^1] = \mathbf{L}\left\{ \sum_{I=1}^{IP} \sum_{J=1}^{IP} 2\mathbf{B}_I^1(\mathbf{x}_L)^{\mathrm{T}}\mathbf{C}\mathbf{B}_J^1(\mathbf{x}_L)|\mathbf{J}|A_L \right\} \tag{51}$$

$$[\mathbf{K}_L^2] = \mathbf{L}\left\{ \sum_{I=1}^{IP} \sum_{J=1}^{IP} \frac{2}{3}\mathbf{B}_I^2(\mathbf{x}_L)^{\mathrm{T}}\mathbf{C}\mathbf{B}_J^2(\mathbf{x}_L)|\mathbf{J}|A_L \right\} \tag{52}$$

which are the contributions of membrane–shear and bending to the stiffness matrix. It is well-known that if a full integration is used in the membrane–shear part ($\mathbf{K}_L^1$ in Equation (51)),

the numerical solution exhibits shear and membrane locking. To remove such locking, nodal integration is employed in $\mathbf{K}_L^1$ and $\mathbf{K}_L^2$, with a strain smoothing introduced to the bending strain of $\mathbf{K}_L^2$. Thus, equivalently, Equation (51) is constructed using a direct nodal integration, whereas Equation (52) is constructed using a SC nodal integration. This formulation resolves locking due to the use of a nodal integration, and the strain smoothing in the bending strain provides stabilization to the nodal integration.

From Equations (46) and (47), the discretized variational equation is obtained as

$$\bar{\mathbf{r}}^{\mathrm{T}}\mathbf{K}\mathbf{r} = \bar{\mathbf{r}}^{\mathrm{T}}\mathbf{F} \tag{53}$$

for all $\bar{\mathbf{r}}$ such that $\bar{\mathbf{z}} = \mathbf{A}\bar{\mathbf{r}} \in Z$. It is difficult to construct the generalized state variable $\bar{\mathbf{r}}$ in kinematically admissible space. $\bar{\mathbf{r}}$ in Equation (53) has to be transformed into physical space to impose an essential boundary condition. Chen *et al.* [30] proposed full transformation, boundary singular kernel, and mixed transformation methods to impose essential boundary conditions in the meshfree method. From numerical experiments, the mixed transformation method may be the most appropriate method in terms of accuracy and efficiency. After imposing the essential boundary condition, the linear system of matrix equations can be solved for $\mathbf{r}$.

5. A UNIFIED DESIGN SENSITIVITY ANALYSIS

In this section, a unified design sensitivity formulation is presented for sizing, shape, and configuration design variables. The sizing design variable (thickness) is treated as part of the shape design variable by defining the sizing design on the solid component level. In addition, the curvature change (configuration design) for the shell structure is considered through the transformation between the physical and parametric co-ordinates. In conjunction with a CAD connection, this approach provides a unique method for representing the design sensitivity coefficient in terms of a design velocity field.

5.1. Material derivative

The first step in DSA is to develop relationships between design variation and the resulting performance measure variations of the structural problem. In the proposed unified design sensitivity approach, all types of designs are related to the structural domain change. Thus, it is convenient to use the material derivative from continuum mechanics to represent the structural domain variation.

The current development in the material derivative approach [31] is based on a linear perturbation of the structural domain in which the material point at the perturbed domain can be expressed in terms of a linear design velocity as

$$\mathbf{x}_\tau = \mathbf{x} + \tau\mathbf{V}(\mathbf{x}) \tag{54}$$

where $\mathbf{V}(\mathbf{x})$ is the design velocity field and τ is a scalar parameter that controls the amount of perturbation.

If the structural domain changes, then the value of state variable $\mathbf{z}(\mathbf{x})$ also changes, in addition to its location of measurement. The point-wise material derivative of state variable

$\mathbf{z}(\mathbf{x})$ is defined as the total variation of $\mathbf{z}_\tau(\mathbf{x}+\tau\mathbf{V})$ in the direction of $\mathbf{V}(\mathbf{x})$, and is evaluated at $\tau=0$ as

$$\dot{\mathbf{z}}=\dot{\mathbf{z}}(\mathbf{x},\mathbf{V})=\left.\frac{\mathrm{d}}{\mathrm{d}\tau}\mathbf{z}_\tau(\mathbf{x}+\tau\mathbf{V})\right|_{\tau=0}=\lim_{\tau\to 0}\left[\frac{\mathbf{z}_\tau(\mathbf{x}+\tau\mathbf{V})-\mathbf{z}(\mathbf{x})}{\tau}\right] \tag{55}$$

Extensive discussion of the material derivative approach is presented in Choi and Haug [31]. It is noted that the domain variation in Equation (55) is defined in the physical domain. However, in this paper, the parametric domain, Ω^r, is independent of any design variables. Thus, only the mapping relation between the physical and parametric domains is a function of the design.

5.2. *Design velocity fields computation*

In this section, a design velocity field is computed for the sizing, shape, and configuration design variables. A unified DSA approach can be made possible by defining a consistent design velocity field that represents all types of design variables. Using the parametric representation of the shell structure in Equation (7), a material point within the structure can be expressed as

$$\mathbf{x}(\xi,\eta,\zeta)=\mathbf{x}^n(\xi,\eta)+\zeta\frac{t}{2}\mathbf{n}(\xi,\eta) \tag{56}$$

A design velocity field is related to the perturbation of this material point in the design direction. In the classical method of categorizing the design variable, a change from t to $t+\tau\delta t$ represents a sizing design variable, whereas a change in $\mathbf{x}^n(\xi,\eta)$ denotes a shape and configuration design variable. In the general curved shell structure, however, it is impossible to distinguish the shape design variable from the configuration design variable.

From the geometric representation in Equation (56), the design velocity field for the shell structure can be written as

$$\mathbf{V}(\xi,\eta,\zeta)=\mathbf{V}^n(\xi,\eta)+\zeta\frac{\delta t}{2}\mathbf{n}(\xi,\eta) \tag{57}$$

where $\mathbf{V}^n(\xi,\eta)$ represents the design velocity of the neutral surface and $\delta t(\xi,\eta)$ denotes the thickness variation. Accordingly, $\delta t(\xi,\eta)$ is related to the sizing design, and $\mathbf{V}^n(\xi,\eta)$ is related to the shape and configuration design.

The computation of $\mathbf{V}^n(\xi,\eta)$ is directly related to the parametric representation of the neutral surface, as given in Equation (1). If only one design variable u is considered for the sake of simplicity, the design dependence of the neutral surface is written as

$$\mathbf{x}^n(u)=\mathbf{U}(\xi)^{\mathrm{T}}\mathbf{M}\mathbf{G}(u)\mathbf{M}^{\mathrm{T}}\mathbf{W}(\eta) \tag{58}$$

Since geometric matrix $\mathbf{G}(u)$ is a function of the design u, the design velocity $\mathbf{V}^n(\xi,\eta)$ can be obtained by perturbing u to $u+\tau\delta u$, and then differentiating with respect to τ as

$$\begin{aligned}\mathbf{V}^n(\xi,\eta)&=\left.\frac{\mathrm{d}\mathbf{x}^n(u+\tau\delta u)}{\mathrm{d}\tau}\right|_{\tau=0}\\&=\mathbf{U}(\xi)^{\mathrm{T}}\mathbf{M}\left(\frac{\partial\mathbf{G}}{\partial u}\delta u\right)\mathbf{M}^{\mathrm{T}}\mathbf{W}(\eta)\end{aligned} \tag{59}$$

For example, when the x-component of $\mathbf{p}_{00}$ is chosen as the design variable u, then matrix $\partial\mathbf{G}/\partial u$ has all zero components except for the component at $(1,1)$ that has a value of [1, 0, 0], if $\delta u = 1$.

In this case, the design velocity field $\mathbf{V}(\xi,\eta,\zeta)$ obtained in Equation (57) corresponds to one design variable u. For the following derivations, only one design variable will be considered for simplicity.

An advantage of the design velocity computation in Equation (57) is that it is unnecessary to store design velocity $\mathbf{V}$ for every particle point. It is instead enough to store matrix $\partial\mathbf{G}/\partial u$ and δt for each design variable. Note that $\partial\mathbf{G}/\partial u$ does not change during the optimization process.

5.3. *Material derivative formulas*

In this section, useful material derivative formulas, which are related to the design sensitivity formulation, will be developed. Since the parametric co-ordinate is independent of design perturbation, the order of differentiation can be exchanged. This property will be used in the following derivations.

Since the Jacobian matrix in Equation (9) relates the physical co-ordinate to the parametric co-ordinate, it is dependent on the design. The material derivative of the Jacobian matrix can be obtained as

$$\frac{\mathrm{d}}{\mathrm{d}\tau}\mathbf{J}_\tau\bigg|_{\tau=0} = \frac{\mathrm{d}}{\mathrm{d}\tau}\left(\frac{\partial\mathbf{x}_\tau}{\partial\boldsymbol{\xi}}\right)\bigg|_{\tau=0} = \frac{\partial\mathbf{V}}{\partial\boldsymbol{\xi}} \tag{60}$$

and the material derivative of its inverse can also be obtained, by using $\mathbf{J}\mathbf{J}^{-1} = \mathbf{I}$, as

$$\frac{\mathrm{d}}{\mathrm{d}\tau}\mathbf{J}_\tau^{-1}\bigg|_{\tau=0} = \frac{\mathrm{d}}{\mathrm{d}\tau}\left(\frac{\partial\boldsymbol{\xi}}{\partial\mathbf{x}_\tau}\right)\bigg|_{\tau=0} = -\mathbf{J}^{-1}\frac{\partial\mathbf{V}}{\partial\mathbf{x}} \tag{61}$$

Finally, the determinant of Jacobian depends on the design, whose material derivative can be obtained from the direct calculation [32] as

$$\frac{\mathrm{d}}{\mathrm{d}\tau}|\mathbf{J}_\tau|\bigg|_{\tau=0} = \frac{\partial V_i}{\partial\xi_i}|\mathbf{J}| = \operatorname{div}\mathbf{V}|\mathbf{J}| \tag{62}$$

When a surface traction force is applied, surface integration is involved in the structural analysis. As the domain shape changes, the surface Jacobian matrix depends on the design. Choi and Haug [31] developed the material derivative of this surface Jacobian matrix in the continuum formulation. A similar process can be used to obtain the material derivative of the surface Jacobian matrix, by presuming that the reference geometry is the parametric domain. However, to simplify the explanation, this complex derivation is not presented in this paper. In addition to the Jacobian matrix, the direction cosine vectors in Equation (10) and unit vectors $\mathbf{S}^1$ and $\mathbf{S}^2$ in Equation (36) explicitly depend on design variable u. The material derivative formulas for these variables are developed in the appendix.

A performance measure for the shell structure is usually defined on the neutral surface, which can be transformed into the parametric domain, as described in Equation (14). After this transformation, a structural performance measure may be written in integral form as

$$\psi = \iint_{\Omega^r} g(\mathbf{z},u)|\mathbf{J}|\,\mathrm{d}\Omega^r \tag{63}$$

Function g is assumed to be continuously differentiable with respect to its arguments. The functional form of Equation (63) represents a variety of structural performance measures. For example, the structural volume can be written with g depending only on u; the averaged stress over a subset of a shell can be written in terms of u and z; and the displacement at a point can be formally written using the Dirac-δ measure and z within the integrand.

Since the parametric domain Ω^r is independent of the design perturbation, the integral in Equation (63) is interchangeable with the design differentiation. Thus, differentiating the functional with respect to design u gives

$$\begin{aligned}\psi' &= \frac{\mathrm{d}}{\mathrm{d}\tau}\left[\iint_{\Omega^r} g(\mathbf{z}_\tau(\mathbf{x}+\tau\mathbf{V}), u+\tau\delta u)|\mathbf{J}_\tau|\,\mathrm{d}\Omega^r\right]\Bigg|_{\tau=0} \\ &= \iint_{\Omega^r} (g_{,\mathbf{z}}^{\mathrm{T}}\dot{\mathbf{z}} + g\,\mathrm{div}\,\mathbf{V} + g_{,u}\delta u)|\mathbf{J}|\,\mathrm{d}\Omega^r \end{aligned} \tag{64}$$

The chain rule of differentiation, along with the definition in Equation (55) has been used to calculate the integrand in Equation (64). The objective here is to obtain an explicit expression of ψ' in terms of δu, which requires rewriting the first term under the integral on the right of Equation (64) explicitly in terms of δu.

5.4. Direct differentiation method

The direct differentiation method computes the first integrand on the right-hand side of Equation (64) by directly computing $\dot{\mathbf{z}}$ from the structural Equation (22). Since this equation satisfies for all design ranges, we can differentiate it with respect to the design variable. To that end, the structural bilinear form is differentiated as

$$\frac{\mathrm{d}}{\mathrm{d}\tau}a(\mathbf{z},\bar{\mathbf{z}})\bigg|_{\tau=0} \equiv a(\dot{\mathbf{z}},\bar{\mathbf{z}}) + a'_V(\mathbf{z},\bar{\mathbf{z}}) \tag{65}$$

where $a(\dot{\mathbf{z}},\bar{\mathbf{z}})$ is the same as in Equation (19) by substituting $\mathbf{z}$ into $\dot{\mathbf{z}}$, and provides the implicitly dependent terms on the design through $\dot{\mathbf{z}}$. $a'_V(\mathbf{z},\bar{\mathbf{z}})$ represents the explicitly dependent terms on the design.

The explicit expression of $a'_V(\mathbf{z},\bar{\mathbf{z}})$ depends on the shell formulation used in the structural problem, which will be derived as follows. The material derivative for the membrane–shear strain tensor can be obtained from its definition in Equation (17) and from the formula in Equation (61) as

$$\begin{aligned}\frac{\mathrm{d}}{\mathrm{d}\tau}(\varepsilon^1_{ij}(\mathbf{z}))\bigg|_{\tau=0} &= \frac{\mathrm{d}}{\mathrm{d}\tau}\left(\mathrm{sym}\left(\frac{\partial z^1_i}{\partial \xi_m}J^{-1}_{mi} + z^2_i J^{-1}_{3j}\right)\right)\bigg|_{\tau=0} \\ &= \mathrm{sym}\left(\frac{\partial \dot{z}^1_i}{\partial x_j} + \dot{z}^2_i J^{-1}_{3j}\right) - \mathrm{sym}\left(\frac{\partial z^1_i}{\partial x_m}\frac{\partial V_m}{\partial x_j} + z^2_i J^{-1}_{3m}\frac{\partial V_m}{\partial x_j}\right) \\ &\equiv \varepsilon^1_{ij}(\dot{\mathbf{z}}) + \varepsilon^{V1}_{ij}(\mathbf{z}) \end{aligned} \tag{66}$$

In Equation (66), $\varepsilon_{ij}^{1}(\dot{\mathbf{z}})$ implicitly depends on the design through $\dot{\mathbf{z}}$ and $\varepsilon_{ij}^{V1}(\mathbf{z})$ represents the explicitly dependent part that can be computable from both the given analysis result $\mathbf{z}$ and the design velocity $\mathbf{V}$. Similarly, the material derivative for the bending strain becomes

$$\left.\frac{\mathrm{d}}{\mathrm{d}\tau}(\varepsilon_{ij}^{2}(\mathbf{z}))\right|_{\tau=0} = \mathrm{sym}\left(\frac{\partial \dot{z}_i^2}{\partial x_j}\right) - \mathrm{sym}\left(\frac{\partial z_i^1}{\partial x_m}\frac{\partial V_m}{\partial x_j}\right)$$
$$\equiv \varepsilon_{ij}^{2}(\dot{\mathbf{z}}) + \varepsilon_{ij}^{V2}(\mathbf{z}) \tag{67}$$

The constitutive relation in Equation (44) explicitly depends on the design, since the transformation between the local co-ordinate and the global co-ordinate is a function of the design. As the neutral surface geometry changes, the direction of the local co-ordinate also changes from the relation described in Equation (11). Thus, this explicit dependency of the constitutive relation can be calculated as

$$\mathbf{C}(u) = \mathbf{Q}(u)^{\mathrm{T}}\mathbf{D}\mathbf{Q}(u) \tag{68}$$

$$\mathbf{C}^{V}(u) = \dot{\mathbf{Q}}^{\mathrm{T}}\mathbf{D}\mathbf{Q} + \mathbf{Q}^{\mathrm{T}}\mathbf{D}\dot{\mathbf{Q}} \tag{69}$$

where $\dot{\mathbf{Q}}$ is the material derivative of the transformation matrix in Equation (45), which can easily be obtained by using Equations (A1)–(A3) given in the appendix.

By using Equations (62), (66), (67) and (69), the explicitly dependent term of the structural energy form $a'_V(\mathbf{z}, \bar{\mathbf{z}})$ can be calculated as

$$\begin{aligned}
a'_V(\mathbf{z},\bar{\mathbf{z}}) = {} & 2\iint_{\Omega^r} \varepsilon_{ij}^{V1}(\bar{\mathbf{z}})C_{ijkl}\varepsilon_{kl}^{1}(\mathbf{z})|\mathbf{J}|\,\mathrm{d}\Omega^r \\
& + 2\iint_{\Omega^r} \varepsilon_{ij}^{1}(\bar{\mathbf{z}})C_{ijkl}\varepsilon_{kl}^{V1}(\mathbf{z})|\mathbf{J}|\,\mathrm{d}\Omega^r \\
& + 2\iint_{\Omega^r} \varepsilon_{ij}^{1}(\bar{\mathbf{z}})C_{ijkl}^{V}\varepsilon_{kl}^{1}(\mathbf{z})|\mathbf{J}|\,\mathrm{d}\Omega^r \\
& + 2\iint_{\Omega^r} \varepsilon_{ij}^{1}(\bar{\mathbf{z}})C_{ijkl}\varepsilon_{kl}^{1}(\mathbf{z})\,\mathrm{div}\,\mathbf{V}|\mathbf{J}|\,\mathrm{d}\Omega^r \\
& + \frac{2}{3}\iint_{\Omega^r} \varepsilon_{ij}^{V2}(\bar{\mathbf{z}})C_{ijkl}\varepsilon_{kl}^{2}(\mathbf{z})|\mathbf{J}|\,\mathrm{d}\Omega^r \\
& + \frac{2}{3}\iint_{\Omega^r} \varepsilon_{ij}^{2}(\bar{\mathbf{z}})C_{ijkl}\varepsilon_{kl}^{V2}(\mathbf{z})|\mathbf{J}|\,\mathrm{d}\Omega^r \\
& + \frac{2}{3}\iint_{\Omega^r} \varepsilon_{ij}^{2}(\bar{\mathbf{z}})C_{ijkl}^{V}\varepsilon_{kl}^{2}(\mathbf{z})|\mathbf{J}|\,\mathrm{d}\Omega^r \\
& + \frac{2}{3}\iint_{\Omega^r} \varepsilon_{ij}^{2}(\bar{\mathbf{z}})C_{ijkl}\varepsilon_{kl}^{2}(\mathbf{z})\,\mathrm{div}\,\mathbf{V}|\mathbf{J}|\,\mathrm{d}\Omega^r
\end{aligned} \tag{70}$$

Even though Equation (70) looks complicated, every term appears systematically. Note that $a'_V(\mathbf{z}, \bar{\mathbf{z}})$ is linear in δu.

The load linear form in Equation (21) is also differentiable with respect to the design. More specifically, for design independent f^{B}, the explicitly dependent term of the load linear form is

$$\left.\frac{\mathrm{d}}{\mathrm{d}\tau}\ell(\bar{\mathbf{z}})\right|_{\tau=0} = 2\iint_{\Omega^r} \bar{\mathbf{z}}^{\mathrm{T}}\mathbf{f}^{\mathrm{B}}\,\mathrm{div}\,\mathbf{V}|\mathbf{J}|\,\mathrm{d}\Omega^r \equiv \ell'_V(\bar{\mathbf{z}}) \tag{71}$$

Since a conservative load is assumed, the load linear form in Equation (71) does not have any implicitly dependent term. As in the case of the energy bilinear form, the variation of the load linear form is linear in δu. If the concentrated, constant load is applied to the structure, then variation of the load linear form in Equation (71) vanishes.

For the direct differentiation method of DSA, one may take the variation of both sides of Equation (22), and use Equations (65) and (71) to obtain the design sensitivity equation as

$$a(\dot{\mathbf{z}}, \bar{\mathbf{z}}) = \ell'_V(\bar{\mathbf{z}}) - a'_V(\mathbf{z}, \bar{\mathbf{z}}), \quad \forall \bar{\mathbf{z}} \in Z \tag{72}$$

Presuming that state variable $\mathbf{z}$ is known as the solution to Equation (22), Equation (72) is a variational equation for the first variation $\dot{\mathbf{z}}$ and has the same energy bilinear form. Since Equation (72) can be solved directly for $\dot{\mathbf{z}}$, it is called the *direct differentiation method* compared to the adjoint variable method, which will be discussed in the next section. Noting that the right-hand side of Equation (72) is a linear form in $\bar{\mathbf{z}} \in Z$, and that the energy bilinear form on the left-hand side is Z-elliptic, Equation (72) has a unique solution, $\dot{\mathbf{z}}$ [31]. The fact that there is a unique solution agrees with the previously stated observation that a design derivative exists for the solution to the state equation. After solving Equation (72) for $\dot{\mathbf{z}}$, the sensitivity of ψ can be calculated from Equation (64).

5.5. *Adjoint variable method*

An adjoint variable method computes the implicitly dependent term, i.e. the first integral on the right-hand side of Equation (64), by defining an adjoint equation. The adjoint equation is introduced by replacing $\dot{\mathbf{z}}$ in Equation (64) with a virtual displacement $\bar{\boldsymbol{\lambda}}$, and by equating the terms involving $\bar{\boldsymbol{\lambda}}$ in Equation (64) to energy bilinear form $a(\boldsymbol{\lambda}, \bar{\boldsymbol{\lambda}})$, yielding the *adjoint equation* for the *adjoint variable* $\boldsymbol{\lambda}$

$$a(\boldsymbol{\lambda}, \bar{\boldsymbol{\lambda}}) = \iint_{\Omega^r} g^{\mathrm{T}}_{,\mathbf{z}}\bar{\boldsymbol{\lambda}}|\mathbf{J}|\,\mathrm{d}\Omega^r, \quad \forall \bar{\boldsymbol{\lambda}} \in Z \tag{73}$$

where a solution $\boldsymbol{\lambda} \in Z$ is desired. To take advantage of the adjoint equation, Equation (73) may be evaluated at $\bar{\boldsymbol{\lambda}} = \dot{\mathbf{z}}$, since $\dot{\mathbf{z}} \in Z$, to obtain

$$a(\boldsymbol{\lambda}, \dot{\mathbf{z}}) = \iint_{\Omega^r} g^{\mathrm{T}}_{,\mathbf{z}}\dot{\mathbf{z}}|\mathbf{J}|\,\mathrm{d}\Omega^r \tag{74}$$

which is the term in Equation (64) that is now needed in order to explicitly write in terms of δu. Similarly, the identity of Equation (72) may be evaluated at $\bar{\mathbf{z}} = \boldsymbol{\lambda}$, since both are in Z, to obtain

$$a(\dot{\mathbf{z}}, \boldsymbol{\lambda}) = \ell'_V(\boldsymbol{\lambda}) - a'_V(\mathbf{z}, \boldsymbol{\lambda}) \tag{75}$$

Recalling that energy bilinear form $a(\bullet,\bullet)$ is symmetrical in its arguments, the left-hand side of Equations (74) and (75) are equal, thus yielding the desired result

$$\iint_{\Omega^r} g_{,\mathbf{z}}^{\mathrm{T}}\dot{\mathbf{z}}\,\mathrm{d}\Omega^r = \ell'_V(\boldsymbol{\lambda}) - a'_V(\mathbf{z},\boldsymbol{\lambda}) \tag{76}$$

where the right-hand side is linear in δu, and can be evaluated once state variable $\mathbf{z}$ and adjoint variable $\boldsymbol{\lambda}$ are determined as solutions to Equations (22) and (73), respectively. Substituting this result into Equation (64), the explicit design sensitivity of ψ is

$$\psi' = \ell'_V(\boldsymbol{\lambda}) - a'_V(\mathbf{z},\boldsymbol{\lambda}) + \iint_{\Omega^r} (g\,\mathrm{div}\,\mathbf{V} + g_{,u}\delta u)|\mathbf{J}|\,\mathrm{d}\Omega^r \tag{77}$$

where the form of the first two terms on the right depends on the problem under investigation.

5.6. *Meshfree discretization*

To numerically compute the design sensitivity coefficient, the design sensitivity equation has to be discretized in the same way as for the structural analysis: using either Equation (72) for the direct differentiation method, or Equation (73) for the adjoint variable method. For this purpose, it is necessary to discretize $a'_V(\mathbf{z},\bar{\mathbf{z}})$ and $\ell'_V(\bar{\mathbf{z}})$ consistently with the method employed in Section 4.3. In this section, a meshfree discretization for the design sensitivity equation is discussed.

In the solid structure, meshfree interpolation function $\Psi_I(\mathbf{x})$ is constructed on physical domain Ω, whose shape is a design variable. Thus, $\Psi_I(\mathbf{x})$ is a function of the design variable. However, since the $\Psi_I(\boldsymbol{\xi})$ in Equation (31) is calculated on a parametric domain Ω^r that is independent of the design, $\Psi_I(\boldsymbol{\xi})$ is also independent of the design. This is a quite different result when compared to the previous development of DSA for the solid structure [33]. In the case of the shell structure, design dependence is established through the Jacobian matrix in Equation (60).

Even if $\Psi_I(\boldsymbol{\xi})$ is independent of the design, the displacement approximation in Equation (35) has explicitly dependent terms on design through thickness t as well as through unit vectors $\mathbf{S}^1$ and $\mathbf{S}^2$. This explicit dependence is denoted as

$$\mathbf{z}^{\mathrm{fic}} = \sum_{I=1}^{IP} \Psi_I(\xi,\eta)\frac{\delta t}{2}\zeta[\mathbf{S}_I^{1^{\mathrm{T}}}, -\mathbf{S}_I^{2^{\mathrm{T}}}]\begin{bmatrix}\alpha_I\\ \beta_I\end{bmatrix} + \sum_{I=1}^{IP} \Psi_I(\xi,\eta)\frac{t}{2}\zeta[\dot{\mathbf{S}}_I^{1^{\mathrm{T}}}, -\dot{\mathbf{S}}_I^{2^{\mathrm{T}}}]\begin{bmatrix}\alpha_I\\ \beta_I\end{bmatrix} \tag{78}$$

where the expressions of $\dot{\mathbf{S}}_I^1$ and $\dot{\mathbf{S}}_I^2$ are provided in Equations (A6) and (A7) in the appendix. By using Equation (78), $\varepsilon_{ij}^{V1}(\mathbf{z})$ in Equation (66) and $\varepsilon_{ij}^{V2}(\mathbf{z})$ in Equation (67) can be discretized as

$$\boldsymbol{\varepsilon}^{V1}(\mathbf{z}) = \mathbf{S}_q\mathbf{T}^V\sum_{I=1}^{IP}\mathbf{G}_I^1\mathbf{r}_I + \mathbf{S}_q\mathbf{T}\sum_{I=1}^{IP}\mathbf{G}_I^{V1}\mathbf{r}_I \equiv \sum_{I=1}^{IP}\mathbf{B}_I^{V1}\mathbf{r}_I \tag{79}$$

$$\boldsymbol{\varepsilon}^{V2}(\mathbf{z}) = \mathbf{S}_q\mathbf{T}^V\sum_{I=1}^{IP}\mathbf{G}_I^2\mathbf{r}_I + \mathbf{S}_q\mathbf{T}\sum_{I=1}^{IP}\mathbf{G}_I^{V2}\mathbf{r}_I \equiv \sum_{I=1}^{IP}\mathbf{B}_I^{V2}\mathbf{r}_I \tag{80}$$

where

$$\mathbf{G}_I^{V1} = \frac{1}{2}\Psi_I \begin{bmatrix} 0 & 0 & 0 & 0 & 0 \\ 0 & 0 & 0 & 0 & 0 \\ 0 & 0 & 0 & (\delta t_I S_{Ix}^1 + t_I \dot{S}_{Ix}^1) & -(\delta t_I S_{Ix}^2 + t_I \dot{S}_{Ix}^2) \\ 0 & 0 & 0 & 0 & 0 \\ 0 & 0 & 0 & 0 & 0 \\ 0 & 0 & 0 & (\delta t_I S_{Iy}^1 + t_I \dot{S}_{Iy}^1) & -(\delta t_I S_{Iy}^2 + t_I \dot{S}_{Iy}^2) \\ 0 & 0 & 0 & 0 & 0 \\ 0 & 0 & 0 & 0 & 0 \\ 0 & 0 & 0 & (\delta t_I S_{Iz}^1 + t_I \dot{S}_{Iz}^1) & -(\delta t_I S_{Iz}^2 + t_I \dot{S}_{Iz}^2) \end{bmatrix} \tag{81}$$

$$\mathbf{G}_I^{V2} = \frac{1}{2} \begin{bmatrix} 0 & 0 & 0 & \Psi_{I,\xi}(\delta t_I S_{Ix}^1 + t_I \dot{S}_{Ix}^1) & -\Psi_{I,\xi}(\delta t_I S_{Ix}^2 + t_I \dot{S}_{Ix}^2) \\ 0 & 0 & 0 & \Psi_{I,\eta}(\delta t_I S_{Ix}^1 + t_I \dot{S}_{Ix}^1) & -\Psi_{I,\eta}(\delta t_I S_{Ix}^2 + t_I \dot{S}_{Ix}^2) \\ 0 & 0 & 0 & 0 & 0 \\ 0 & 0 & 0 & \Psi_{I,\xi}(\delta t_I S_{Iy}^1 + t_I \dot{S}_{Iy}^1) & -\Psi_{I,\xi}(\delta t_I S_{Iy}^2 + t_I \dot{S}_{Iy}^2) \\ 0 & 0 & 0 & \Psi_{I,\eta}(\delta t_I S_{Iy}^1 + t_I \dot{S}_{Iy}^1) & -\Psi_{I,\eta}(\delta t_I S_{Iy}^2 + t_I \dot{S}_{Iy}^2) \\ 0 & 0 & 0 & 0 & 0 \\ 0 & 0 & 0 & \Psi_{I,\xi}(\delta t_I S_{Iz}^1 + t_I \dot{S}_{Iz}^1) & -\Psi_{I,\xi}(\delta t_I S_{Iz}^2 + t_I \dot{S}_{Iz}^2) \\ 0 & 0 & 0 & \Psi_{I,\eta}(\delta t_I S_{Iz}^1 + t_I \dot{S}_{Iz}^1) & -\Psi_{I,\eta}(\delta t_I S_{Iz}^2 + t_I \dot{S}_{Iz}^2) \\ 0 & 0 & 0 & 0 & 0 \end{bmatrix} \tag{82}$$

$$\mathbf{T}_I^V = \begin{bmatrix} \mathbf{J}^{-1}\dfrac{\partial \mathbf{V}}{\partial \mathbf{x}} & \mathbf{0} & \mathbf{0} \\ \mathbf{0} & \mathbf{J}^{-1}\dfrac{\partial \mathbf{V}}{\partial \mathbf{x}} & \mathbf{0} \\ \mathbf{0} & \mathbf{0} & \mathbf{J}^{-1}\dfrac{\partial \mathbf{V}}{\partial \mathbf{x}} \end{bmatrix}_I \tag{83}$$

Since the structural problem is solved for the generalized state variable $\mathbf{r}$ the strain vectors in Equations (79) and (80) can be calculated easily at $\mathbf{x}_L$. $a'_V(\mathbf{z}, \bar{\mathbf{z}})$ in Equation (70), and $\ell'_V(\bar{\mathbf{z}})$ in Equation (71) can be discretized as

$$a'_V(\mathbf{z}, \bar{\mathbf{z}}) \approx \bar{\mathbf{r}}^{\mathrm{T}} \mathbf{F}^a \tag{84}$$

$$\ell'_V(\bar{\mathbf{z}}) \approx \bar{\mathbf{r}}^{\mathrm{T}} \mathbf{F}^\ell \tag{85}$$

where

$$\mathbf{F}^a = \sum_{L=1}^{NP} \mathbf{F}_L^a \tag{86}$$

$$\mathbf{F}^{\ell} = \sum_{L=1}^{NP} \mathbf{F}_L^{\ell} \tag{87}$$

$$\mathbf{F}_L^a = \mathbf{L}\left\{ \sum_{I=1}^{IP} 2[\mathbf{B}_I^{V1^{\mathrm{T}}}\mathbf{C}\boldsymbol{\varepsilon}^1 + \mathbf{B}_I^{1^{\mathrm{T}}}\mathbf{C}\boldsymbol{\varepsilon}^{V1} + \mathbf{B}_I^{1^{\mathrm{T}}}(\mathbf{C}^V + \mathbf{C}\,\mathrm{div}\,\mathbf{V})\boldsymbol{\varepsilon}^1]|\mathbf{J}|\,A_L \right\}$$
$$+ \mathbf{L}\left\{ \sum_{I=1}^{IP} \frac{2}{3}[\mathbf{B}_I^{V2^{\mathrm{T}}}\mathbf{C}\boldsymbol{\varepsilon}^2 + \mathbf{B}_I^{2^{\mathrm{T}}}\mathbf{C}\boldsymbol{\varepsilon}^{V2} + \mathbf{B}_I^{2^{\mathrm{T}}}(\mathbf{C}^V + \mathbf{C}\,\mathrm{div}\,\mathbf{V})\boldsymbol{\varepsilon}^2]|\mathbf{J}|\,A_L \right\} \tag{88}$$

$$\mathbf{F}_L^{\ell} = \mathbf{L}\left\{ \sum_{I=1}^{IP} 2(\Psi_I \mathbf{f}^{\mathrm{B}}\,\mathrm{div}\,\mathbf{V})|\mathbf{J}|\,A_L \right\} \tag{89}$$

The discretized design sensitivity equation for the direct differentiation method is

$$\bar{\mathbf{r}}^{\mathrm{T}}\mathbf{K}\dot{\mathbf{r}} = \bar{\mathbf{r}}^{\mathrm{T}}(\mathbf{F}^{\ell} - \mathbf{F}^a) \tag{90}$$

for all $\bar{\mathbf{r}}$ such that $\bar{\mathbf{z}} = \mathbf{A}\bar{\mathbf{r}} \in Z$. Note that the stiffness matrix of Equation (90) is the same as that of Equation (53). Thus, the L–U factorized stiffness matrix from structural analysis can be used for solving the sensitivity Equation (90) with a different right-hand side. This property increases the efficiency of DSA, as shown in Section 6. After computing $\dot{\mathbf{r}}, \dot{\mathbf{z}}$ can be computed from the relations in Equations (35) and (78), from which ψ' in Equation (64) can be computed.

In the adjoint variable method, the adjoint load in Equation (73) has to be discretized, as

$$\iint_{\Omega^r} g_{,\mathbf{z}}^{\mathrm{T}}\,\bar{\boldsymbol{\lambda}}|\mathbf{J}|\,\mathrm{d}\Omega^r \approx \bar{\boldsymbol{\eta}}^{\mathrm{T}}\mathbf{F}^{\mathrm{adj}} \tag{91}$$

By using this adjoint load, the adjoint matrix equation is obtained, as

$$\bar{\boldsymbol{\eta}}^{\mathrm{T}}\mathbf{K}\boldsymbol{\eta} = \bar{\boldsymbol{\eta}}^{\mathrm{T}}\mathbf{F}^{\mathrm{adj}} \tag{92}$$

for all $\bar{\boldsymbol{\eta}}$ such that $\bar{\boldsymbol{\lambda}} = \mathbf{A}\bar{\boldsymbol{\eta}} \in Z$. After computing the adjoint vector $\boldsymbol{\eta}$, the adjoint variable $\boldsymbol{\lambda}$ can be obtained from $\boldsymbol{\lambda} = \mathbf{A}\boldsymbol{\eta}$, and then the sensitivity of the performance measure can be obtained from Equation (77). In the adjoint variable method, the computation of $\boldsymbol{\eta}$ in Equation (92) exclusively depends on the performance measure. Thus, the matrix Equation (92) is solved once for each performance measure and Equation (77) is repeatedly calculated for each design variable.

6. NUMERICAL EXAMPLES

6.1. Size design sensitivity analysis for a plate

In this section, a size DSA is considered for the simple plate-bending problem, in order to compare the sensitivity accuracy with the analytical solution. Figure 5 shows a clamped plate with a concentrated force at the centre point. Table I shows the parameters used in meshfree analysis. To see the convergent behaviour of the sensitivity results, four different models are considered for meshfree discretization, i.e. 5×5, 9×9, 13×13, and 17×17 particles. Since the geometry and boundary conditions are symmetrical, only a quarter of the plate is modelled.

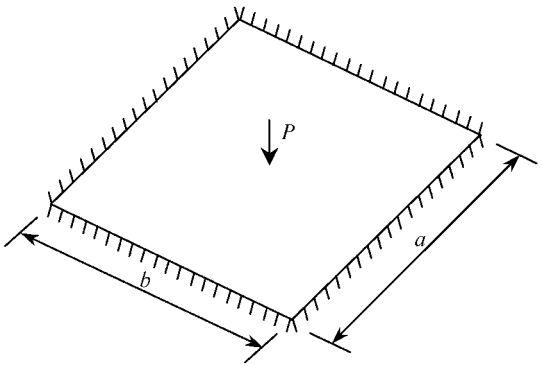

Figure 5. Clamped plate bending problem with concentrated load.

Table I. Meshfree analysis parameters.

Parameters	Value
Young's modulus E	3×10^6
Poisson's ratio v	0.3
Plate dimension	80×80
Plate thickness t	0.8
Boundary condition	Clamped
Applied force P	1.0 (vertical)
Kernel function	Cubic spline
Normalized dilation parameter (a_x, a_y)	(2.0, 2.0)
Completeness condition	First order

The analytical solution for centre point deflection can be found in the literature [34]. For the case of the clamped, rectangular plate, the maximum deflection appears at the centre of the plate whose magnitude is

$$z_{\max} = \alpha \frac{Pa^2}{D} \tag{93}$$

where a is the function of a/b, i.e. the ratio of the plate dimension and D is the flexural rigidity, defined as

$$D = \frac{Et^3}{12(1 - v^2)} \tag{94}$$

Since this analytical solution is the explicit function of plate thickness, the analytical design sensitivity for centre point deflection can easily be obtained. From Equations (93) and (94), it is clear that centre point deflection is a function of plate thickness through the flexural rigidity. Thus, the sizing design sensitivity of Equation (93) can be obtained as

$$\dot{z}_{\max} = -\alpha \frac{3Pa^2}{Dt} \tag{95}$$

The design sensitivity result of the proposed method is then compared with the analytical design sensitivity in Equation (95) for different particle distribution densities. Figure 6 plots

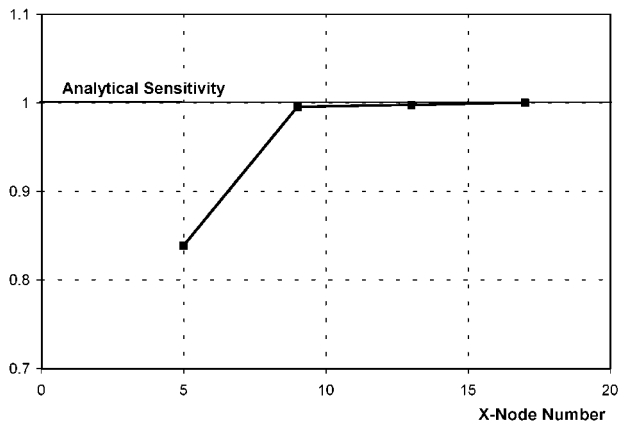

Figure 6. Design sensitivity convergence of centre point deflection.

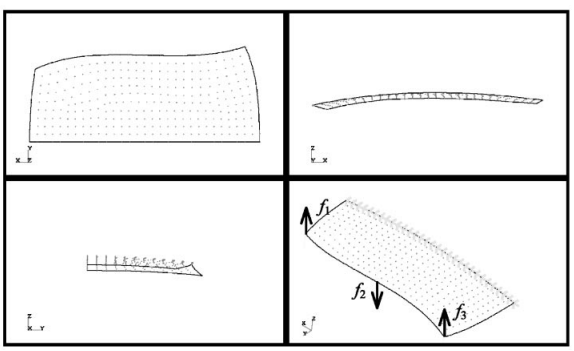

Figure 7. Meshfree discretization of a vehicle roof model.

the convergent behaviour of normalized design sensitivity results. The proposed design sensitivity method yields almost exactly the same result after 13×13 discretization. Centre point deflection also shows a similar convergent behaviour.

6.2. Design sensitivity analysis of a vehicle roof

For a real application of the shell design problem, consider a vehicle roof structure, as shown in Figure 7. Only half of the roof structure is modelled using a single spline surface with a PATRAN geometric modeller [24]. A total of 347 meshfree particles are distributed on the surface, which corresponds to 1735 degrees-of-freedom. A linear elastic material property is assumed with a Young's modulus $E = 26\,000$ MPa, and a Poisson's ratio $v = 0.3$. A constant thickness $t = 2$ mm is used. To evaluate the bending rigidity, three point loads are applied at each pillar location, as described in Figure 7 with $f_1 = 100$ kN, $f_2 = -200$ kN and $f_3 = 100$ kN.

The first step in a meshfree analysis is to compute the nodal area. For a given set of particle distributions, a Voronoi diagram [22] can be used to compute the nodal area, which

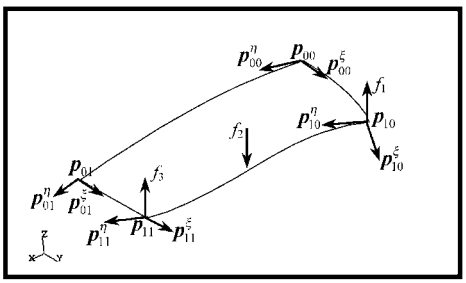

Figure 8. Design parameterization of the roof structure.

Table II. Design parameterization.

ID	Design description
1	Vertical movement of $\mathbf{p}^{\xi}_{00}$
2	Vertical movement of $\mathbf{p}^{\xi}_{10}$
3	Vertical movement of $\mathbf{p}^{\xi}_{01}$
4	Vertical movement of $\mathbf{p}^{\xi}_{11}$
5	Vertical movement of $\mathbf{p}^{\eta}_{00}$
6	Vertical movement of $\mathbf{p}^{\eta}_{10}$
7	Vertical movement of $\mathbf{p}^{\eta}_{01}$
8	Vertical movement of $\mathbf{p}^{\eta}_{11}$
9	Applied force f_1
10	Applied force f_2
11	Applied force f_3
12	Young's modulus E
13	Poisson's ratio v

will act as the integration weight. The meshfree shape function is computed in the parametric domain by imposing the reproducing condition, and the smoothed strain is then obtained from Equation (34). The domain integration is carried out at each particle point in order to construct the stiffness matrix. After imposing the essential boundary condition, the linear matrix equation is solved by using the LAPACK package [35]. For DSA purposes, the factorized stiffness matrix is retained. Plate 1 plots the von Mises stress contour at the shell surface.

All components of the geometric matrix in Equation (3) can be treated as shape/configuration design variables. In this specific example, the vertical movement of the tangent vectors is considered as a design variable, such that the curvature of the roof can be changed. In addition, non-conventional design variables such as the material property (Young's modulus and Poisson's ratio), and the applied load are considered. Figure 8 illustrates the definitions of geometric matrix **G**, while Table II shows the design variables of the roof structure. A total of 13 design variables are chosen for DSA purposes, which include eight shape/configuration designs, three applied load designs, and two material property designs.

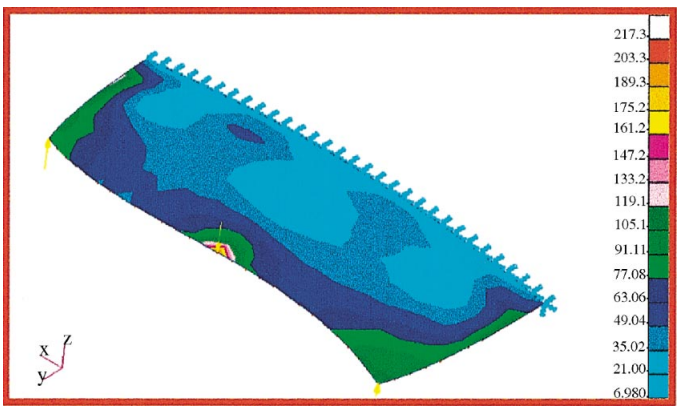

Plate 1. Meshfree analysis results (stress plot).

Table III. Computational cost for meshfree analysis and sensitivity computation.

Activity	CPU + IO (s)
Data input and nodal volume	1.8
Shape function computation	1.46
Stiffness matrix	24.7
Essential boundary condition	0.43
Matrix solution	8.54
DSA per performance measure	0.94

Since the adjoint variable method is more efficient than the direct differentiation method for many design problems, the former method is used for this example. Eight performance measures are chosen that include the structural volume and the seven von Mises stresses. Since the volume performance measure does not require any adjoint equation, seven adjoint equations are solved by using a factorized stiffness matrix from the structural analysis. Again, it is important to stress that the number of adjoint equations is related to the number of performance measures, rather than the number of design variables. The computational costs of DSA include the computation of adjoint load $\mathbf{F}^{\text{adj}}$, the solution procedure of adjoint Equation (92), and the evaluation of the sensitivity in Equation (77). A very efficient design sensitivity computation is achieved, as is summarized in Table III. The last row in Table III represents the DSA cost of a performance measure for 13 design variables, which is about 2.5 per cent of the total structural analysis cost. This kind of efficiency can be obtained since the proposed method does not require any stiffness matrix derivative, so that the adjoint equation is solved simply, using a back-substitution of the factorized matrix.

The accuracy of the proposed DSA is compared with the FDM in Table IV. The first column in Table IV denotes the type of performance measure (volume and stresses), while the second column represents their values in the original design. It is well known that the selection of the perturbation size $\Delta\tau$ is a major difficulty in FDM. Given the fact that the solution has an accuracy of at least about six numerical digits, perturbation size is chosen such that the performance change $\Delta\psi$ is about 10^{-6} times the performance value, as shown in the third column. The fourth column represents the predicted design change by using the method proposed by Equation (77). This predicted design change is compared with the finite difference $\Delta\psi$ in the last column. Very accurate sensitivity results are obtained, as shown throughout Table IV.

7. CONCLUSION

A unified development of design sensitivity analysis has been presented for the shell structure with respect to the sizing, shape, and configuration design variables by using the meshfree method. Useful information from CAD geometry is used in the shear-deformable, meshfree shell formulation. The design velocity field is defined in the solid component level, and is then degenerated by following the same degeneration process for the shell structure. Very efficient and accurate sensitivity results are obtained and are compared with finite difference results with excellent agreement.

Table IV. Accuracy of sensitivity results.

Type	ψ	$\Delta\psi$	$\psi'\Delta\tau$	$(\Delta\psi/\psi'\Delta\tau)\times 100$
(a) u_1, $\Delta\tau = 1.602\text{E}-02$				
Volume	1.51033E+06	1.95212E − 01	1.95180E − 01	100.02
σ_{169}	1.34898E+02	9.43339E − 03	9.43429E − 03	99.99
σ_{182}	2.17291E+02	8.96848E − 03	8.96976E − 03	99.99
σ_{195}	1.35578E+02	7.27985E − 03	7.28063E − 03	99.99
σ_{17}	1.21676E+02	1.32524E − 03	1.32552E − 03	99.98
σ_{31}	1.09005E+02	2.88250E − 03	2.88289E − 03	99.99
σ_{301}	8.66971E+01	2.66191E − 03	2.66156E − 03	100.01
σ_{302}	7.34885E+01	1.72660E − 03	1.72636E − 03	100.01
(b) u_3, $\Delta\tau = 1.354\text{E}-02$				
Volume	1.51033E+06	2.08691E − 01	2.08665E − 01	100.01
σ_{169}	1.34898E+02	6.58233E − 03	6.58289E − 03	99.99
σ_{182}	2.17291E+02	7.80610E − 03	7.80689E − 03	99.99
σ_{195}	1.35578E+02	7.50906E − 03	7.50947E − 03	99.99
σ_{17}	1.21676E+02	2.64271E − 04	2.64279E − 04	100.00
σ_{31}	1.09005E+02	7.37644E − 04	7.37657E − 04	100.00
σ_{301}	8.66971E+01	4.77743E − 03	4.77783E − 03	99.99
σ_{302}	7.34885E+01	1.06057E − 03	1.06138E − 03	99.92
(c) u_{10}, $\Delta\tau = 3.793\text{E}-03$				
Volume	1.51033E+06	0.00000E+00	0.00000E+00	0.00
σ_{169}	1.34898E+02	−2.12311E − 03	−2.12310E − 03	100.00
σ_{182}	2.17291E+02	−3.52794E − 03	−3.52793E − 03	100.00
σ_{195}	1.35578E+02	−2.11374E − 03	−2.11373E − 03	100.00
σ_{17}	1.21676E+02	−1.37942E − 04	−1.37941E − 04	100.00
σ_{31}	1.09005E+02	1.94032E − 05	1.94029E − 05	100.00
σ_{301}	8.66971E+01	−1.72318E − 04	−1.72319E − 04	100.00
σ_{302}	7.34885E+01	−9.10049E − 05	−9.10035E − 05	100.00
(d) u_{13}, $\Delta\tau = 1.853\text{E}-05$				
Volume	1.51033E+06	0.00000E+00	0.00000E+00	0.00
σ_{169}	1.34898E+02	3.98915E − 04	3.98709E − 04	100.05
σ_{182}	2.17291E+02	6.15776E − 04	6.15426E − 04	100.06
σ_{195}	1.35578E+02	3.67303E − 04	3.66965E − 04	100.09
σ_{17}	1.21676E+02	−4.93757E − 05	−4.93850E − 05	99.98
σ_{31}	1.09005E+02	−2.60711E − 05	−2.60801E − 05	99.97
σ_{301}	8.66971E+01	3.88180E − 04	3.87581E − 04	100.15
σ_{302}	7.34885E+01	1.02153E − 03	1.02096E − 03	100.06

APPENDIX

As the shape and the configuration of the shell structure change, the direction cosines of the local co-ordinate also change. However, this dependence is explicit on the design. From their definitions in Equation (10), the material derivatives of these direction cosines are

calculated as

$$\dot{\mathbf{l}} = \frac{\mathrm{d}}{\mathrm{d}\tau}\left(\frac{\mathbf{x}^n_{,\xi}}{\|\mathbf{x}^n_{,\xi}\|}\right)$$

$$= \frac{1}{\|\mathbf{x}^n_{,\xi}\|}(\mathbf{I} - \mathbf{l}\otimes\mathbf{l})\dot{\mathbf{x}}^n_{,\xi} \tag{A1}$$

$$\dot{\mathbf{n}} = \frac{\mathrm{d}}{\mathrm{d}\tau}\left(\frac{\mathbf{x}^n_{,\xi}\times\mathbf{x}^n_{,\eta}}{\|\mathbf{x}^n_{,\xi}\times\mathbf{x}^n_{,\eta}\|}\right)$$

$$= \frac{1}{\|\mathbf{x}^n_{,\xi}\times\mathbf{x}^n_{,\eta}\|}[\mathbf{I} - \mathbf{n}\otimes\mathbf{n}](\dot{\mathbf{x}}^n_{,\xi}\times\mathbf{x}^n_{,\eta} + \mathbf{x}^n_{,\xi}\times\dot{\mathbf{x}}^n_{,\eta}) \tag{A2}$$

$$\dot{\mathbf{m}} = \dot{\mathbf{n}}\times\mathbf{l} + \mathbf{n}\times\dot{\mathbf{l}} \tag{A3}$$

where the design dependent terms $\dot{\mathbf{x}}^n_{,\xi}$ and $\dot{\mathbf{x}}^n_{,\eta}$ can be computed from their definitions in Equations (5) and (6) as

$$\dot{\mathbf{x}}^n_{,\xi} = \mathbf{U}_{,\xi}(\xi)^{\mathrm{T}}\mathbf{M}\left(\frac{\partial\mathbf{G}}{\partial u}\delta u\right)\mathbf{M}^{\mathrm{T}}\mathbf{W}(\eta) \tag{A4}$$

$$\dot{\mathbf{x}}^n_{,\eta} = \mathbf{U}(\xi)^{\mathrm{T}}\mathbf{M}\left(\frac{\partial\mathbf{G}}{\partial u}\delta u\right)\mathbf{M}^{\mathrm{T}}\mathbf{W}_{,\eta}(\eta) \tag{A5}$$

Since matrix $\partial\mathbf{G}/\partial u$ is supplied by the design parameterization, Equations (A4) and (A5) are explicitly represented as linear functions of design perturbation δu.

In addition, the directions that define the rotational angle of the deformation depends on the design, from their definitions in Equation (36), as

$$\dot{\mathbf{S}}^1 = \dot{\mathbf{n}}\times\mathbf{e}_1 \tag{A6}$$

$$\dot{\mathbf{S}}^2 = \dot{\mathbf{n}}\times\mathbf{S}^1 + \mathbf{n}\times\dot{\mathbf{S}}^1 \tag{A7}$$

where the expression of $\dot{\mathbf{n}}$ is given in Equation (A2).

ACKNOWLEDGEMENTS

This research is supported by General Motors and NSF/DARPA Optimized Portable Algorithms of Applications Libraries (OPAAL). This support is gratefully acknowledged.

REFERENCES

1. Zyczkowski M. Recent advances in optimal structural design of shells. *European Journal of Mechanics and Solids* 1992; **11**:5–24.
2. Botkin ME. Shape optimization of plate and shell structures. *AIAA Journal* 1982; **20**:268–273.
3. Gates AA, Accorsi ML. Automatic shape optimization of three-dimensional shell structures with large shape change. *Computers and Structures* 1993; **49**:167–178.

4. Lee SJ, Hinton E. Dangers inherited in shells optimized with linear assumptions. *Computers and Structures* 2000; **78**:473–486.
5. Csonka B, Kozak I, Mota Soares CM, Mota Soares CA. Shape optimization of axisymmetric shells using a higher-order shear deformation theory. *Structural Optimization* 1995; **9**:117–127.
6. Oral S. A Mindlin plate finite element with semi-analytical shape design sensitivities. *Computers and Structures* 2000; **78**:467–472.
7. Chenis D. Discrete gradient and discretized continuum gradient methods for shape optimization of shells. *Mechanics of Structures and Machines* 1994; **22**:73–115.
8. Lindby T, Santos JLT. Shape optimization of three-dimensional shell structures with the shape parameterization of a CAD system. *Structural Optimization* 1999; **18**:126–133.
9. Choi KK, Shim I, Wang S. Design sensitivity analysis of structure-induced noise and vibration. *ASME Journal of Vibration and Acoustics* 1997; **119**:173–179.
10. Choi B, Park YH, Choi KK. Shape design sensitivity analysis of a joint mechanism using a doubly-curved shell. *Computers and Structures* 2000; **77**:495–507.
11. Moita JS, Infante Barbosa J, Mota Soares CM, Mota Soares CA. Sensitivity analysis and optimal design of geometrically non-linear laminated plates and shells. *Computers and Structures* 2000; **76**:407–420.
12. Barthelemy BM, Chon CT, Haftka RT. Accuracy problems associated with semi-analytical derivatives of static response. *Finite Element Analysis and Design* 1988; **4**:249–265.
13. Pugh EDL, Hinton E, Zienkiewicz OC. A study of quadrilateral plate bending element with reduced integration. *International Journal for Numerical Methods in Engineering* 1978; **12**:1059–1079.
14. Hughes TJR. *Finite Element Method.* Prentice-Hall: Englewood Cliffs, NJ, 1987.
15. Bathe KJ, Dvorkin EN. A four-node plate bending element based on Mindlin/Reissner plate theory and a mixed interpolation. *International Journal for Numerical Methods in Engineering* 1985; **21**:367–383.
16. Belytschko T, Wong BK. Assumed strain stabilization procedure for the 9-node Lagrange shell element. *International Journal for Numerical Methods in Engineering* 1989; **28**:385–414.
17. Murthy SS, Gallagher RH. A triangular thin-shell finite element based on discrete Kirchhoff theory. *Computer Methods in Applied Mechanics and Engineering* 1986; **54**:197–222.
18. Krysl P, Belytschko T. Analysis of thin shells by the element-free Galerkin method. *International Journal of Solids and Structures* 1996; **33**:3057–3080.
19. Donning B, Liu WK. Meshless methods for shear-deformable beams and plates. *Computer Methods in Applied Mechanics and Engineering* 1998; **152**:47–72.
20. Garcia O, Fancello EA, Barcellos CS, Duarte CA. hp-Clouds in Mindlin's thick plate model. *International Journal for Numerical Methods in Engineering* 2000; **47**:1381–1400.
21. Noguchi H, Hawashima T, Miyamura T. Element free analysis of shell and spatial structures. *International Journal for Numerical Methods in Engineering* 2000; **47**:1215–1240.
22. Chen JS, Wu CT, Yoon S, You Y. Stabilized conforming nodal integration for Galerkin meshfree methods. *International Journal for Numerical Methods in Engineering* 2000; **50**(2):435–466.
23. Liu WK, Jun S, Zhang YF. Reproducing kernel particle methods. *International Journal for Numerical Methods in Fluids* 1995; **20**:1081–1106.
24. *MSC/PATRAN User's Guide*. The MacNeal-Schwendler Corp., 1999.
25. Chang KH, Choi KK, Tsai CS, Chen CJ, Choi BS, Yu X. Design sensitivity analysis and optimization tool (DSO) for shape design applications. *Computing Systems in Engineering* 1995; **6**:151–175.
26. Shames IH, Dym CL. *Energy and Finite Element Methods in Structural Mechanics*. McGraw-Hill: New York, 1996.
27. Reissner E. The effect of transverse shear deformation on the bending of elastic plates. *ASME Journal of Applied Mechanics* 1945; **12**:A69–A77.
28. Mindlin RD. Influence of rotary and shear deformation on flexural motions of isotropic plates. *ASME Journal of Applied Mechanics* 1952; **18**:31–38.
29. Bathe KJ. *Finite Element Procedures*. Prentice-Hall: Englewood Cliffs, NJ, 1996.
30. Chen JS, Wang HP. New boundary condition treatments for meshless computation of contact problems. *Computer Methods in Applied Mechanics and Engineering* 2000; **187**:441–468.
31. Choi KK, Haug EJ. Shape design sensitivity analysis of elastic structures. *Journal of Structural Mechanics* 1983; **11**:231–269.
32. Arora JS, Lee TH, Cardoso JB. Structural shape sensitivity analysis: relationship between material derivative and control volume approaches. *AIAA Journal* 1992; **36**:1638–1648.
33. Kim NH, Choi KK, Park YH, Chen JS. Meshless shape design sensitivity analysis and optimization for contact problem with friction. *Computational Mechanics* 2000; **25**:157–168.
34. Timoshenko SP, Woinowsky-Krieger S. *Theory of Plates and Shells* (2nd edn). McGraw-Hill: New York.
35. Anderson E, Bai Z, Bischof C, Blackford S, Demmel J, Dongarra J, Du Croz J, Greenbaum A, Hammarling S, McKenney A, Sorensen D. *LAPACK User's Guide* (3rd edn). SIAM: Philadelphia, 1999.

